POLITECNICO DI TORINO

Master's Degree in Mechanical Engineering

Experimental measurements to extract friction contact parameters for aero-engine applications

Candidate:
CRISTIANA PENNISI

Supervisors:
PROF. STEFANO ZUCCA
PROF. DANIELE BOTTO

ACADEMIC YEAR 2018-2019

“God made the bulk;

surfaces were invented by the devil”

Wolfgang Pauli

Abstract

Aircraft gas turbines are characterized by thousands of mechanical joints (e.g. bolted joints, dove-tail and fir-tree joints) connecting components together. These joints introduce frictional contacts because contact interfaces suffer from relative (sliding) motion due to vibrations. Unfortunately, these frictional contacts are a major source of uncertainty for the correct prediction of the dynamic response of assembled structures: in fact, they introduce strong nonlinearities due to the nonlinear nature of the friction force. A great deal of research is currently being conducted to better understand and model the nonlinear frictional behaviour of joints.

This study focuses on the underlying physics of friction and on the two major parameters used in the nonlinear friction contact models: the friction coefficient and the tangential contact stiffness. In particular, the aim of this study is to experimentally investigate the evolution of such contact parameters during the wear process, identifying possible dependencies on external factors, such as excitation frequency, normal load and sliding distance.

Table of contents

List of Figures

List of Tables

Nomenclature

μ	Friction coefficient
k_t	Contact stiffness [N/µm]
N	Normal load [N]
T	Friction force [N]
x, d	Relative displacement [µm]
E	Energy dissipated [J]
V_p	Volume of the peaks [μm^3]
V_h	Volume of the holes [μm^3]
$V_{loss,fix}$	Worn volume lost from the fixed specimen [$\mu m \cdot mm^2$]
$V_{loss,mob}$	Worn volume lost from the mobile specimen[$\mu m \cdot mm^2$]
V_{loss}	Total volume loss from the pair of specimens [$\mu m \cdot mm^2$]

Chapter 1

1. Introduction

Thousands of mechanical joints can be found in aircraft gas turbines (Figure 1), such as bolted joints, dove-tail and fir-tree joints, connecting components together. In correspondence of these joints, contact interfaces suffer from sliding motion due to vibrations, thus introducing friction.

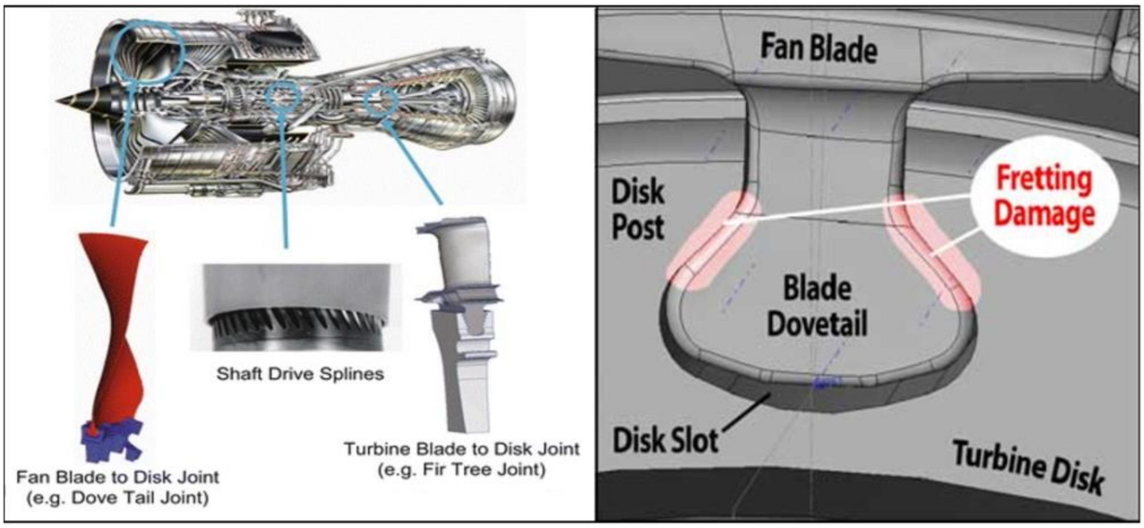

Figure 1 a) Mechanical joints in aero engines [1]; b) Fretting damage region in a dove-tail joint

The prediction of friction forces and energy dissipations occurring at the contact surfaces is of the utmost importance; in fact, these strongly affect the dynamic behaviour of the structure in terms of stiffness and damping. If they are not adequately monitored, they may lead to catastrophic failures at the jointed interfaces due to high cycle fatigue.

To predict and avoid these potential failures, a correct analysis of the turbine dynamic response is fundamental. Unfortunately, frictional contacts occurring at vibrating contact interfaces introduce strong nonlinearities due to the nonlinear nature of friction forces. As a consequence, contact models are required that can replicate physical phenomena occurring at the contact interfaces and allow to predict the friction forces required for the dynamic analysis.

The two major contact parameters used as input in such contact models are the friction coefficient and the contact stiffness. These contact parameters allow the contact models to recreate the hysteresis loop (Figure 2), which is a plot considered by the research community as the most representative of the underlying physics of the contacting interfaces [2]. It is a cyclic load-deflection curve that plots the friction force against the relative displacement occurring between two oscillating contact interfaces.

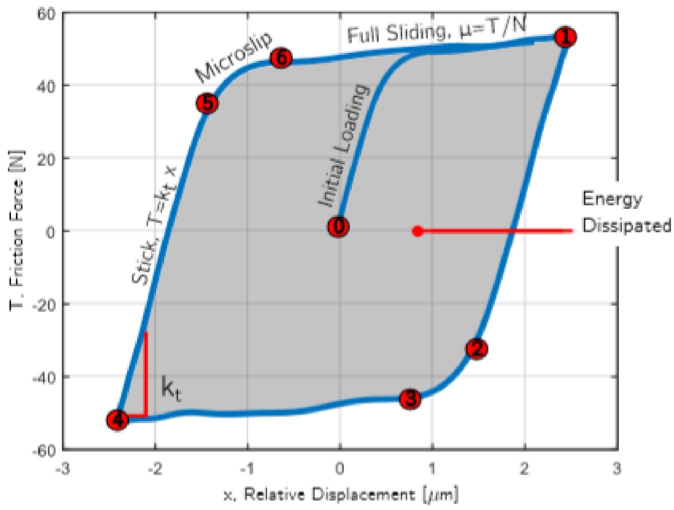

Figure 2 An example of hysteresis loop [3]

The friction coefficient μ defines the limit at which the contact starts to slide: when the contact tangential force becomes constant and equal to the friction limit (T=μN, where

N is the normal load that presses the two bodies together), the whole area of contact enters in full sliding.

The contact stiffness is a property of the contacting interfaces and is mainly due to elastic interactions between asperities at the interfaces. It represents the slope of the stick portion of hysteresis loops, where there is a linear relationship between the tangential force and the relative tangential displacement, occurring when the friction force is below the friction limit ($T < \mu N$) and the surfaces are stuck.

The analysis of these two contact parameters is the main objective of this thesis, with the final aim to improve the understanding of the contact for more accurate nonlinear dynamics simulations.

1.1. Objectives

The goal of this study is to improve the current understanding of contact parameters used in traditional contact models by means of an experimental investigation.

The experimental method used in this study consists of hysteresis measurements, based on the recording of hysteresis loops to extract the contact parameters.

A high frequency fretting test rig designed and developed at LAQ AERMEC laboratory of Politecnico di Torino is used to perform the experiments for this study. It is used for measurements of friction contact parameters for industrial applications, such as the aerospace field. The rig embodies a moving specimen that slides over a static one; a constant normal load ensures a continuous contact and a wide range of relative sliding displacement can be imposed.

The main task to be achieved is experimentally identify the behaviour of the contact parameters against variable external factors such as running time, wear, normal load, sliding distances and so on.

1.2. **Outline of the thesis**

This Master Thesis' work is organized as follow:

- Chapter 2 presents an explanation of the different regimes of fretting and a general overview of the physics of both friction coefficient and contact stiffness, by reference to the current literature.
- Chapter 3 contains a detailed description of the high frequency friction rig and of the specimens used for this study.
- In Chapter 4 it is illustrated the method adopted to extract the friction coefficient, the tangential contact stiffness and the dissipated energy from the hysteresis loop and the procedure performed to estimate the worn area of contact and the wear volume lost from the specimens after the fretting process.
- In Chapter 5 the aim of the experimental campaign, the experimental plan and the final results are shown.

Chapter 2

2. Literature review

Friction is the resistance that one surface or object encounters when moving over another. It occurs whenever relative sliding motion takes place between two surfaces and is cause of energy dissipation due to the force transmitted at the contact.

Friction is of particular interest in built-up structures undergoing periodic excitation, where it appears in the form of fretting. The phenomenon of fretting occurs when two bodies get in touch and a low-amplitude vibratory motion takes place between the two surfaces [4].This vibratory motion generates contact tangential forces, which are nonlinear functions of the relative displacement between the two oscillating interfaces. When plotted versus the relative displacement, the friction force might display a straight line, but often displays a "loop", known as hysteresis loop, depending on the contact and operating conditions.

The hysteresis loop is a cyclic load-deflection curve that plots the contact tangential force against the relative displacement occurring between two oscillating contact interfaces.

This curve plays a central role in the modelling of contact and friction. In fact, the research community assumes that hysteresis loops are able to represent to a reasonable degree the underlying physics of the contacting interfaces [2].

Three important pieces of information can be extracted from an hysteresis loop: the contact stiffness, the friction coefficient and the energy dissipated at the contact, as shown in Figure 3.

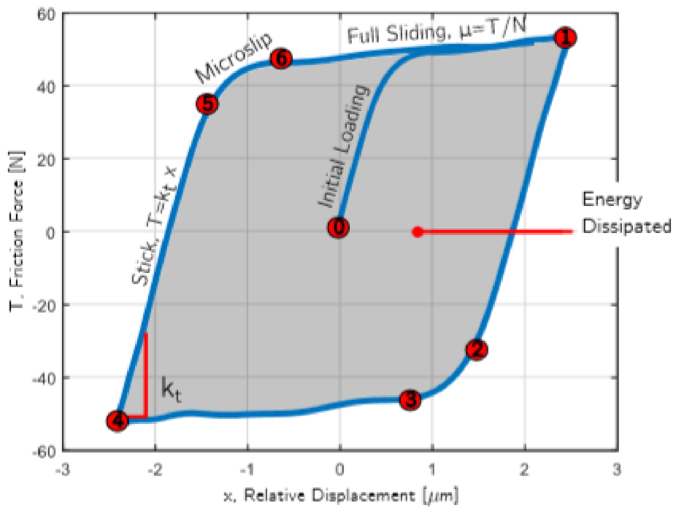

Figure 3 A typical hysteresis loop [3]

When the friction force is below the friction limit defined by Amontons-Coulomb's friction law ($T < \mu N$, where T is the friction force, μ is the friction coefficient and N is the normal load acting on the interfaces), the contact interfaces are stuck (1→2 and 4→5) and the relation between friction force T and relative displacement x is linear; this relation can be expressed, by means of the contact stiffness k_t, as $T = k_t \cdot x$. The contact stiffness is a property of the contacting interfaces mainly due to elastic deformation of the asperities at the interfaces and to the bulk elastic deformation at the macroscopic contact scale. It is modelled as an elastic spring that relates changes in the load with changes in the relative displacement.

When the friction force becomes constant and equal to the friction limit (T=μN), the whole area of contact is in full sliding (3→4 and 6→1). The friction coefficient μ defines the limit at which the contact start to slide.

In the transition between the two contact conditions (2→3 and 5→6), a portion of the area of contact is still stuck (i.e. asperities elastically deform) and the remaining portion start to slip because the friction limit is reached, thus inducing the microslip condition. Furthermore, the total amount of energy dissipated at the contact can be estimated through the area inside the loop. The higher the degree of slipping, the higher the energy dissipation due to the friction force (i.e. the area of the loop is larger).

The mechanisms described above are also shown in Figure 4, with time signals of the friction force and relative displacement.

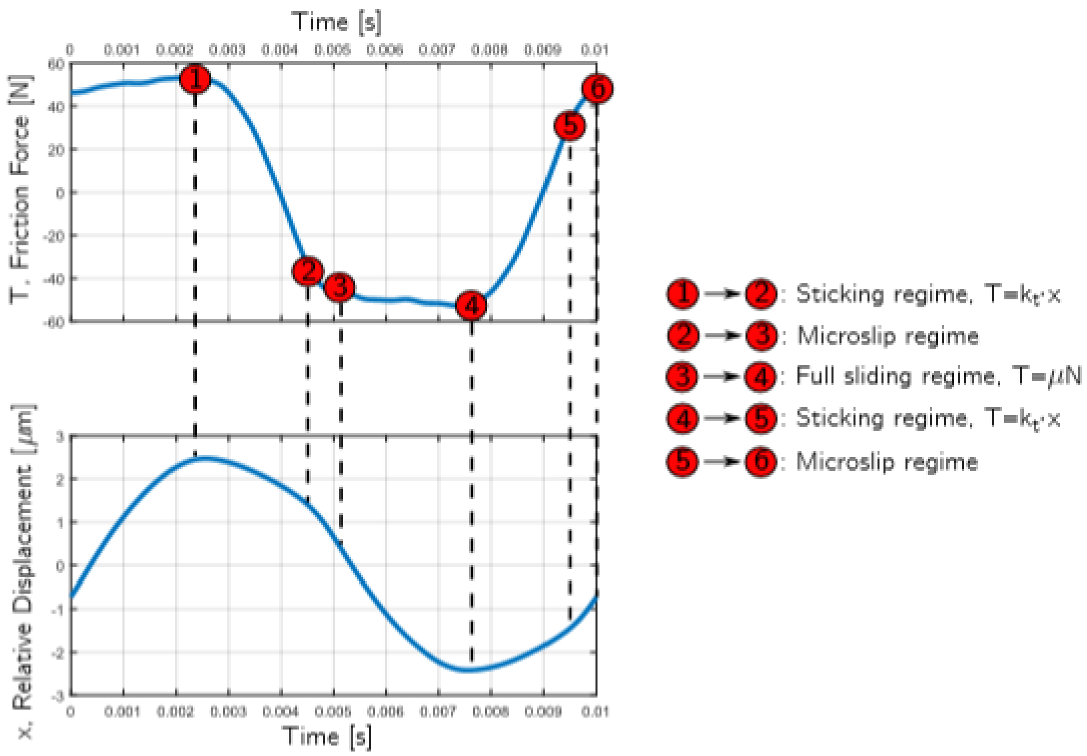

Figure 4 Friction force and relative displacement vs. time

The friction force looks like a square wave due to the fact that during full sliding it reaches the almost constant friction limit. At the same time, the relative displacement varies rapidly during the full sliding and more smoothly during the stick regime since the contact is almost completely stuck.

2.1. Fretting regimes

Since hysteresis loops provide information on the macroscopic behaviour of the two surfaces in contact under a vibratory motion, the analysis of their evolution represent the main tool to investigate the effects of fretting.

In fact, by comparing hysteresis loops with the corresponding damaged surfaces, Vingsbo and Söderberg [5], [6] identified three different regimes of fretting (that occurs with low amplitude oscillatory displacements). Each regime is characterized by a certain amount of surface degradation and its resulting surface appearance, which is correlated to a certain range of displacement amplitudes.

The relevant hysteresis loops are schematically shown in Figure 5. Fretting contact regimes are classified as follows, in ascending order of relative sliding motion [5]:

- Stick regime, which corresponds to low damage fretting. It is marked by very limited surface damage related to corrosion and wear. No fatigue crack nucleation is observed (up to 10^6 cycles).

  As shown in Figure 5a, the tangential force vs. displacement plot for a complete load cycle is a straight line, which indicates predominantly elastic deformation of the asperities and no energy dissipation.

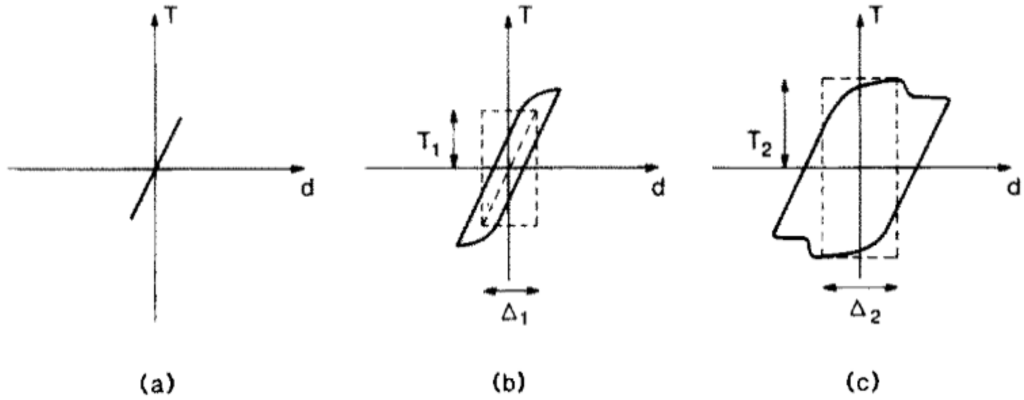

Figure 5 Characteristic examples of tangential force T vs displacement d recordings for different displacement amplitudes Δ [5]. (a) Stick regime. (b) Mixed stick-slip regime. (c) Gross slip regime

- Mixed stick-slip regime, which corresponds to fretting fatigue. This regime is characterized by accelerated growth cracks at the interface that may lead to the degradation of material fatigue properties, whereas wear effects are slight.

  A portion of the area of contact is stuck, while the remaining portion slips. In this case, hysteresis loop presents microslip characteristics, as shown in Figure 5b, and the area of the loop represents the energy dissipated.

- Gross slip regime, which corresponds to fretting wear. This regime involve severe surface damage by oxidation-assisted wear with material removal and debris formation, while crack growth is minimal.

  When the tangential force occurring between the contact interfaces reaches the friction limit, the whole area of contact enters in full sliding and all adhesive asperity contact bridges are broken.

  A sudden drop can be observed in the hysteresis loop shown in Figure 5c; this drop takes place at the "point of incipient gross slip", at which the transition from static friction to dynamic friction occurs ($\mu_{st}>\mu_{din}$).

As explained above, hysteresis loops are characterized by two contact parameters: friction coefficient, μ, and tangential contact stiffness, k_t. In the next paragraphs the physics of friction coefficient and contact stiffness is investigated more in detail.

2.2. Physics of the friction coefficient

The study of friction has a long history. The first recorded scientific study on friction is attributed to Leonardo Da Vinci (1452-1519) [7], who about half a millennium ago formulated the earliest basic statements on friction [8]. These statements turned to be in wholly agreement with the two 'laws' of friction defined 200 years later by the indipendent work of Amontons (1699) [9]. The laws have been defined as follows:

1. **Amontons' first law.** The force of friction T is directly proportional to the applied load N (via the coefficient of friction μ):

$$T = \mu N \tag{1}$$

2. **Amontons' second law.** The force of friction is independent of the "nominal" area of contact.

Later on, in 1785, Coulomb confirmed and extended these findings [10], and introduced a 'third' law of friction stating that kinetic friction is generally lower than static friction and also independent of sliding velocity. Coulomb conducted a systematic work on friction by investigating the influence of several variables on the phenomenon, including the nature of materials in contact, the normal load, the role of asperities and the time of repose. Due to this systematic work, the Amontons' first law is often referred to as Coulomb friction law, whilst it should be called Amontons-Coulomb law of friction. All of the presented laws are based on direct experimental observations, but their physical origin is not fully understood yet. In fact, modern theories of friction are not able to predict accurate values of friction coefficients and even the most recent contact models strikingly still lie on such laws defined centuries ago.

The physical origin of friction has been described in the centuries by adopting three main approaches:

1. Mechanistic approach, based on the concept of the interlocking of asperities.

2. Adhesive approach, based on the concept of cohesive forces arising at the contact.

3. Modern theories based on combined adhesive, deformation and ploughing actions, with the latter two referring respectively to the plastic deformation of asperities and ploughing of wear particles.

The modern theories were born as a result of the limitations presented by the mechanistic and the adhesive approaches. In 1981, Suh and Sin [11] stated that friction is due to three major factors, namely adhesion μ_a, deformation μ_d and ploughing μ_p:

$$\mu = \mu_a + \mu_d + \mu_p \qquad (2)$$

Where:

- μ_a is due to the adhesion forces and is in the range $0 \div 0.4$, where low values are experienced in well-lubricated surfaces, while the highest values occur for identical materials with no contamination or oxide layers. Suh and Sin stated also that in most cases adhesion may not be the dominant factor.
- μ_d is due to the plastic deformation of asperities and is the major source for the static friction coefficient being in the range $0.43 \div 0.75$. During sliding, the actual contribution of asperity deformation is expected to be quite small instead, since frictional resistance is mainly generated by ploughing and adhesion effects.
- μ_p is due to the ploughing of wear particles and is in the range $0 \div 0.4$. Low values are experienced when wear particles are totally absent or when a soft material slides against a harder material (in fact the particles would penetrate in

the softer material and just slide over the harder one). High values are associated to similar mating materials because wear particles may penetrate in both their surfaces, thus increasing the resistance to sliding.

Despite the remarkable advances in the field, a great deal of research is still being conducted to improve the understanding of the physics of friction. A predictive model for the coefficient of friction is not available yet. The main challenge is related to the fact that friction is a complex system with multi-physics and multi-scale aspects, and therefore it cannot be considered as a scalar property. A recent review from the tribology research community emphasized the multi-scale aspects of friction and, more in general, of tribological problems [12]. The multi-physics aspects include plasticity, thermal dissipations, chemical interactions, material pairings, contact geometry and load histories among others, as shown in Figure 6. Furthermore, a predictive model of friction should include multi-scale aspects, bridging length scales from atomistic level to meso-scale levels. For the above mentioned reasons the modelling of friction remains largely empirical and, consequently, the values for the friction coefficient are mainly obtained from experiments.

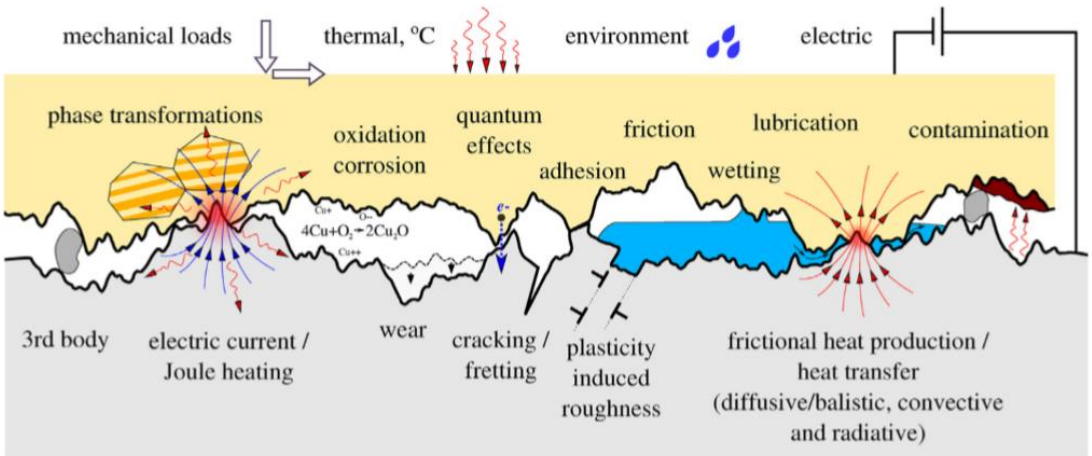

Figure 6 Multi-physics phenomena involved in friction [12]

2.3. **Physics of the contact stiffness**

The contact stiffness is a parameter that linearly relates changes of the load with changes of the relative displacement between the contact interfaces, when the friction force is below the friction limit ($T < \mu N$) and the surfaces are stuck. It represents the slope of the stick portion of hysteresis loops.

The contact stiffness can be defined in both normal and tangential directions. Its physical origin is attributed to the elastic deformation of the asperities coming into contact and to the bulk elastic deformation.

It depends on multiple variables including normal load, surface roughness, wear and area of contact. Several experimental studies investigated the influence of most of these variables. For example, a large variety of experiments has been conducted to investigate the influence of the normal load on the contact stiffness [12]–[21]. A comparison between these different studies is shown in Figure 7.

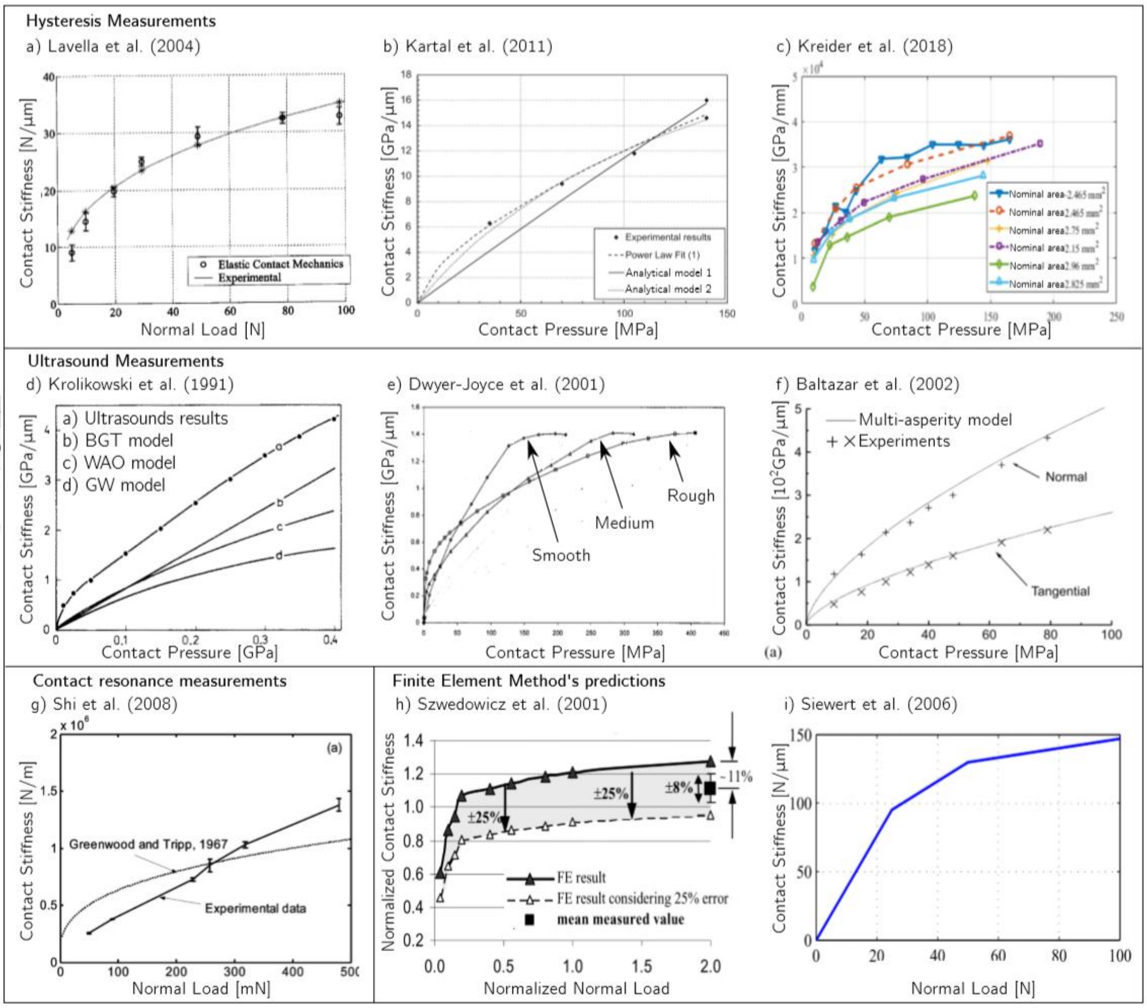

Figure 7 Contact stiffness versus normal load: a-b-c) Hysteresis measurements[20], [23], [31]; d-e-f) Ultrasound measurements [14], [28], [30]; g) Contact resonance measurements [32]; h-i) Finite Element Method predictions [18], [29]

The contact stiffness increases with a high rate for low normal loads and then grows less markedly for moderate and high normal loads. This behaviour is explained by considering the change in the real area of contact. At light loads the contact stiffness is lower because only few asperities come into contact, and therefore the amount of elastic interactions that generate the contact stiffness is limited. As the load increases, more asperities come into contact rapidly, thus contributing to increases in the contact stiffness. At moderate/high loads the contact becomes homogeneously spaced over the whole area, and further increases in the normal load do not affect much the contact stiffness as the number of new contacts is much reduced.

Also the effect of roughness has been investigated in some of these studies, see e.g. Figure 7e [28]. As expected, smooth profiles generates higher contact stiffness values for the same normal load since less load is required to increase the number of contact points. Instead, rough profiles generates lower contact stiffnesses since the asperities' tips largely contribute to the softening of the contact.

The effect of wear has been investigated as well [20], [33]. The contact stiffness increases with fretting cycles until it reaches an asymptotic value. This is probably due to the fact that at the beginning of the tests interfaces are not compliant, and only after several wear cycles the compliance increases thus contributing to the increase in the contact stiffness. However, further investigations are required to improve the current understanding of the effects of wear on both contact stiffness and interface evolution. In particular, it would be interesting to relate the evolution of the interface compliance with the evolution of the contact stiffness, since this aspect isnot considered in most of the existing contact models.

Finally, also the effects of the nominal area of contact have been investigated. It has been confirmed by Finite Element simulations that the contact stiffness is directly proportional to the nominal area of contact [20], [29], and in fact it is a common practice to express it in a normalized form divided by the nominal contact area. However, experimental studies are few [20], and no detailed investigations are present in the current literature.

Chapter 3

3. Hysteresis experimental measurements

Reliable predictions of the dynamic response of built-up structures require to take into account the effect of friction. In fact, frictional contacts occurring at joined vibrating interfaces introduce strong nonlinearities, influencing the dynamic behaviour of the assembly.

Contact models are required that allow to include these nonlinear effects in the dynamic simulations. They replicate physical phenomena occurring at the contact interfaces and allow to predict the friction forces required for the dynamic analysis.

The accuracy of these contact models strongly depends on the provided input parameters. The major contact parameters used as input in such contact models are the friction coefficient and the contact stiffness. These parameters allow the contact models to recreate the hysteresis loop, considered by the research community as the most representative concept of the underlying physics of the contacting interfaces.

Among the different classes of experimental methods adopted to obtain such contact parameters, direct hysteresis measurements are considered the most reliable method to provide input ro recreate hysteresis loops [2].

Hysteresis measurements are in fact based on the recording of hysteresis loops to extract the coefficient of friction and the contact stiffness. In order to experimentally obtain the hysteresis loop, a sliding relative motion has to be generated between two oscillating components, after which two quantities must be measured: the force transmitted between the two sliding components and their relative tangential displacement. In general, forces are measured with force transducers and displacements are measured with contact or non-contact measuring techniques. The hysteresis loop is then obtained by plotting the transmitted friction force versus the relative displacement.

Several friction rigs have been designed at Politecnico di Torino for this purpose. In particular, the flat-on-flat friction rig [34] has been used in this work for hysteresis measurements, and is described in the next section.

3.1. **Description of the test rig**

The test rig is shown in Figure 8. It has been designed and developed in 2010 at the LAQ AERMEC laboratory of the Department of Mechanical and Aerospace Engineering of the Politecnico di Torino [34], [35]. The rig generates a relative oscillatory motion between two specimens in a flat-on-flat arrangement.

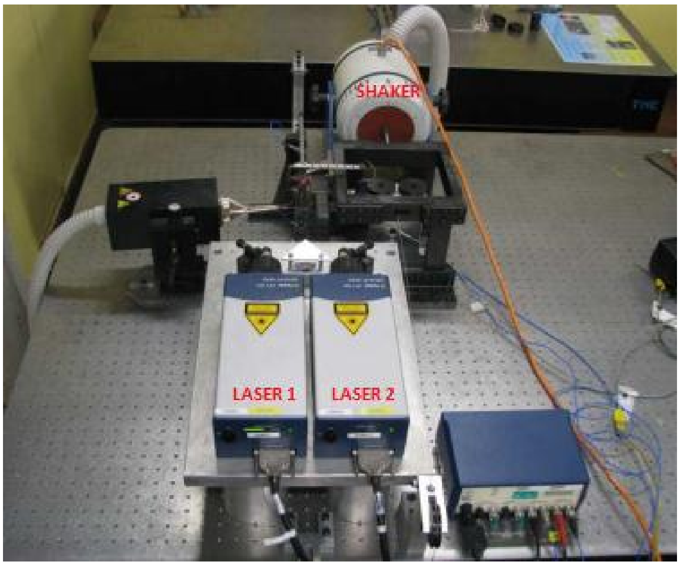

Figure 8 The friction rig [35]

The peculiarity of this rig is the adoption of a floating body approach to bring the surfaces into contact. This kind of approach allows for a self-alignment of the contact interfaces, maximizing the number of contact points between the two surfaces.

3.1.1. The floating body approach

Two approaches can be used in order to bring the two specimens' surfaces into contact: the rigid body and the floating body approach.

With the first method (Figure 9), one body S1 approaches the other one S2 with a translation motion along the z-direction, normal to the contact plane (one degree of freedom). Unfortunately, the two contact surfaces have not the same normal, due to several reasons, including the tolerance of the assembly specimen-test rig, the specimen's surface waviness and the tolerance of the test rig itself. As a result, the initial contact will be in only one point.

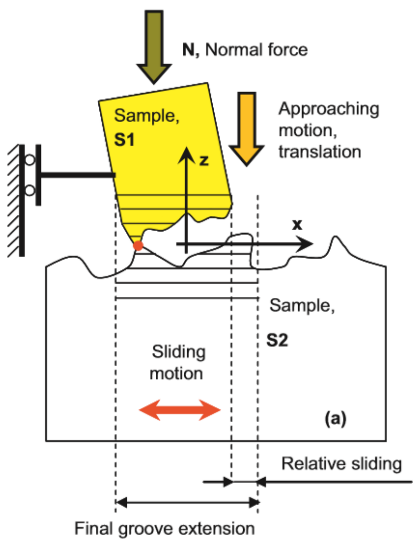

Figure 9 Rigid body approach[34]

Whereas, with the floating body approach (Figure 10), the body S1not only translates towards the other S2 in the z-direction, but it is also left free to rotate around two orthogonal axes, x and y, lying on the contact plane (3 degrees of freedom).

These movements allow to have three contact points and to obtain an actual plane contact.

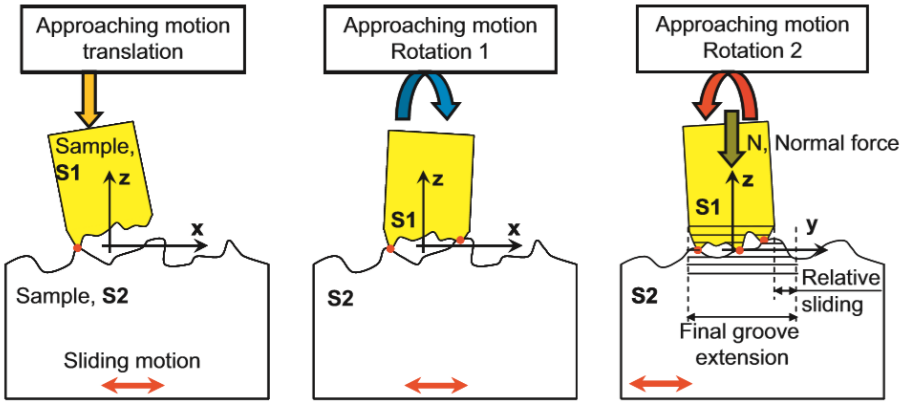

Figure 10 Floating body approach [34]

By using the floating body method, the number of cycles necessary to achieve the stabilized values of contact parameters (which are reached when the area of contact is fully worn) is minimized, because a transient period to extend the point contact to a flat contact is no more required.

3.1.2. The working principle and instrumentation

A model of the test rig is shown in Figure 11.

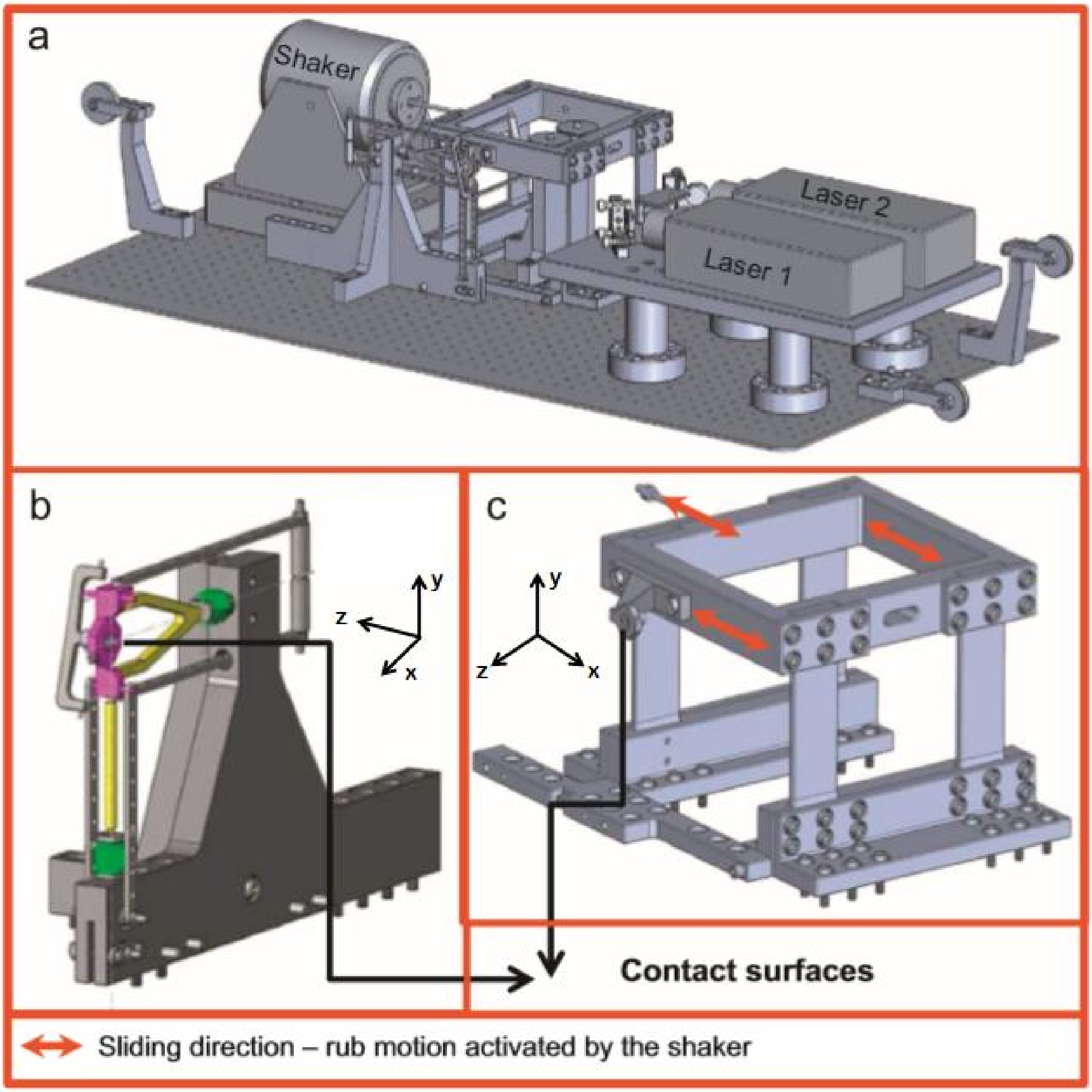

Figure 11 Model of the friction rig [34]: (a) overall view, (b) static side of the rig, (c) moving side of the rig

The two specimens are connected to a static support (in Figure 11b) and a mobile support (in Figure 11c):

- The static support (pink component in Figure 11b) is sustained by two rods (yellow elements) whose ends act on two piezoelectric force transducers (green components) for the measurement of the transmitted tangential force; the rods allow the static support only to rotate around the x and y directions and to translate in the z-direction (floating body approach).

- The mobile support is fixed to an inertial mass which is excited by means of a electrodynamic shaker, providing a sinusoidal excitation (the maximum excitation frequency is 300 Hz).

The mobile specimen slides over the fixed one (Figure 12). Two laser doppler vibrometers (LDVs) measure the velocity of each specimen; the velocity is integrated and the relative displacement obtained by difference. Laser measurement points lie on the edges of the two specimens, as closely as possible to the contact interface. Moreover, contact is constantly ensured by applying a normal load by means of a dead weight and a pulley system.

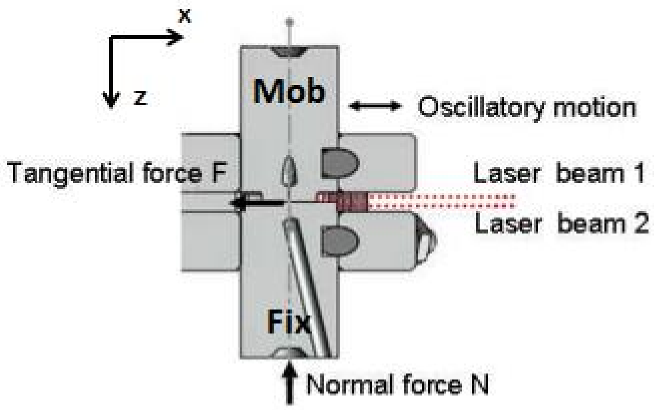

Figure 12 Forces on the contact surfaces [34]

The friction rig is controlled by three input signals (i.e. normal load, excitation frequency and excitation amplitude) and generates two output signals (force and displacement). All the signals are acquired and regulated with a control system, which allows for an instantaneous monitoring of the hysteresis loops. The tangential forces and displacements are stored on file for subsequent data processing. Also temperature at the contact can be measured by means of thermocouples.

3.1.3. The specimens

The rig uses 10mm-diameter cylindrical specimens, as shown in Figure 13.

The contact surfaces of the two specimens, fixed and mobile, have the same width along the sliding motion direction.

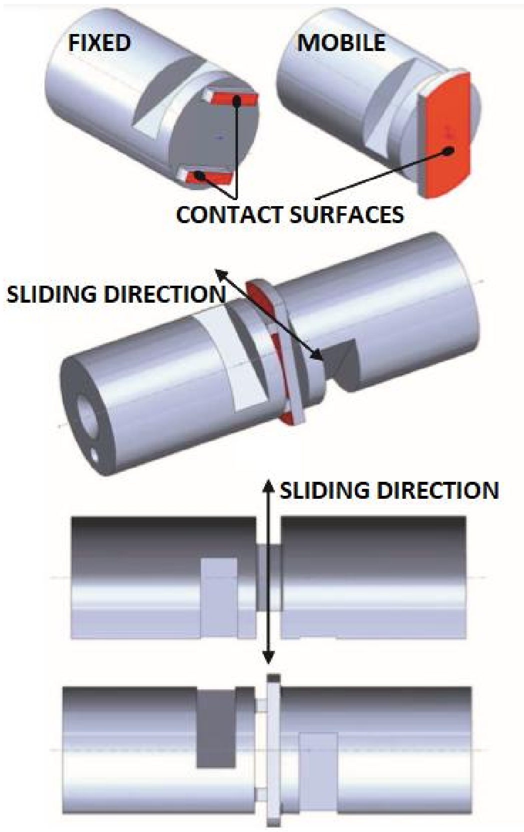

Figure 13 Specimens and contact surfaces [34]

The fixed specimen is characterized by two sliders of the same dimension; this feature allow to have an index of the fretting test repeatability: measuring the worn volumes of the two sliders separately after the fretting test, the same values are expected.

Three different nominal contact areas are considered for this study: 5 mm^2, 10 mm^2 and 40 mm^2; more details are given in the Chapter 5.

Moreover, in both the fixed and the mobile specimen there is a hole through which thermocouples can be introduced in order to measure the temperature of the contact surfaces.

Chapter 4

4. Analysis method

An experimental campaign was conducted at Politecnico di Torino and a wide range of hysteresis loops was recorded under different loading conditions.

After each experiment, the following analysis has been carried out:

- Hysteresis loops were post-processed with Matlab to compute the friction coefficient, the tangential contact stiffness and the dissipated energy during each cycle.
- The specimens used during each run were removed from the test rig and microscope scans of the contact surfaces were performed in order to estimate wear volume and worn area, using the software MountainsMap.

4.1. Friction coefficient and tangential contact stiffness estimation

Three pieces of information can be extracted from the hysteresis loop: friction coefficient, tangential contact stiffness and energy dissipation.

The friction coefficient μ is calculated as the ratio between the friction limit (horizontal portion of the loop) and the applied normal load, according to Amontons-Coulomb's friction law $T = \mu N$. If the tangential contact force during the macroslip phase is not constant, its average value is considered (see blue lines in Figure 14).

The friction coefficient is also calculated using the formulation (3) by means of the energy dissipated during the fretting cycle E, since it represents the area inside the hysteresis loop [34].

$$\mu = \frac{E}{4N\Delta x} \tag{3}$$

Of course, this calculation can only be performed for hysteresis loops in full sliding, and not for loops in a pure stick regime, as the sliding limit is not reached.

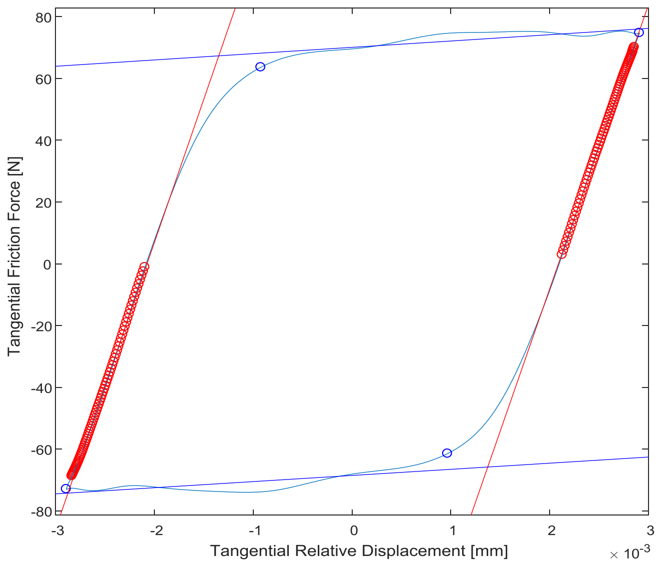

Figure 14 Extraction method of contact parameters from hysteresis loops

The tangential contact stiffness is estimated from the slope of the loop after the reversal of sliding motion (stick portion of the loop), as $T = k_t \cdot x$; it is calculated from both sides of the loops, see red lines in Figure 14. Points used for the interpolation start from the beginning of the reversal of motion up to the 0N value of the friction force.

The dissipated energy is the integral of the area inside the loop.

4.2. **Wear volume loss measurement**

One of the aims of this study is the characterization of the fretting wear mechanisms; the procedure performed to estimate the volume loss during the wear process is explained in detail in this paragraph. Before and after each test the contact surfaces of the specimens were scanned using Alicona – InfiniteFocus instrument based focus variation technology. The interfaces were then given as input to the software MountainsMap for the calculation.

A slightly different approach was used for the two types of specimens, fixed and mobile, as explained below.

Fixed specimen.

The wear volume of the fixed specimen was calculated as the difference between the volumes of the sliders before and after the fretting test (Figure 15). The volume of the sliders was obtained by considering all the material above a reference plane corresponding to the flat plane at the bottom of the sliders.

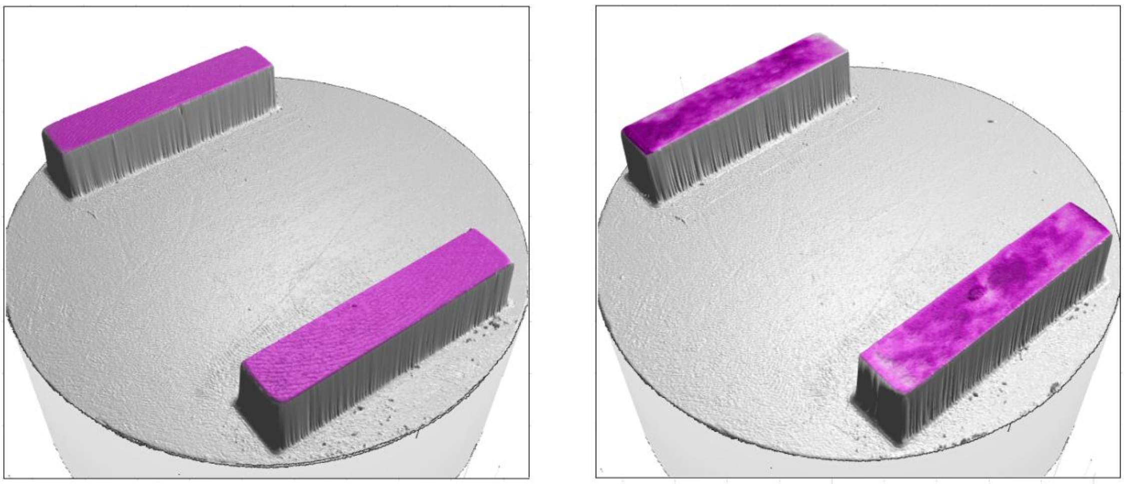

(a) (b)

Figure 15 3D view of a fixed specimen surface: unworn (a); worn (b)

The same procedure was carried out for both the unworn and the worn contact surface of the fixed specimen. For the illustration of the following main steps, an unworn specimen is considered by way of example.

The first step consisted of removing a smooth macroscopic form from the surface outside the contact area, in order to obtain the flat reference plane (black lower surface in Figure 16); then it was levelled removing the tilting.

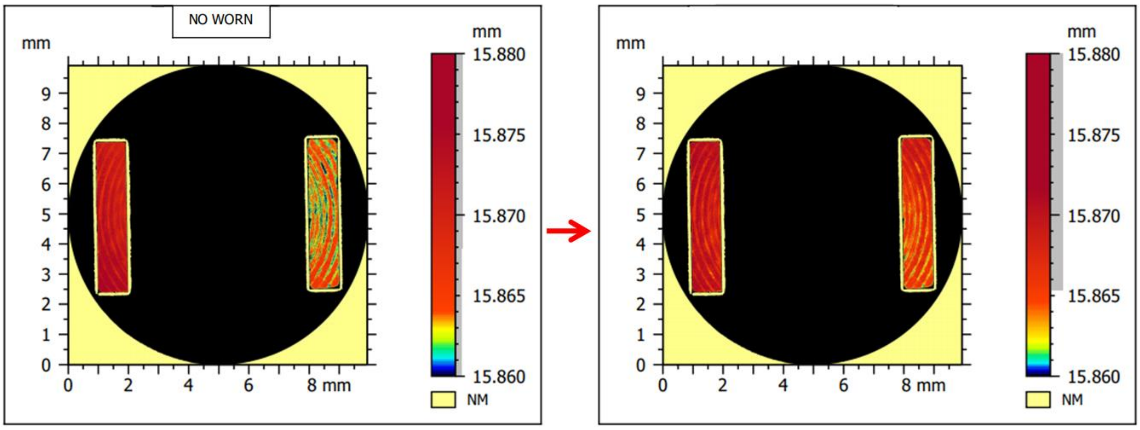

Figure 16 Wear volume analysis of the fixed specimen: remove form and level

After obtaining the flat and levelled reference plane, the two symmetric contact areas (left and right) were extracted in order to calculate the volumes separately, as shown in Figure 17. This operation was obviously carried out only for the specimens with two sliders (i.e. those with nominal contact area of 5 mm^2 and 10 mm^2).

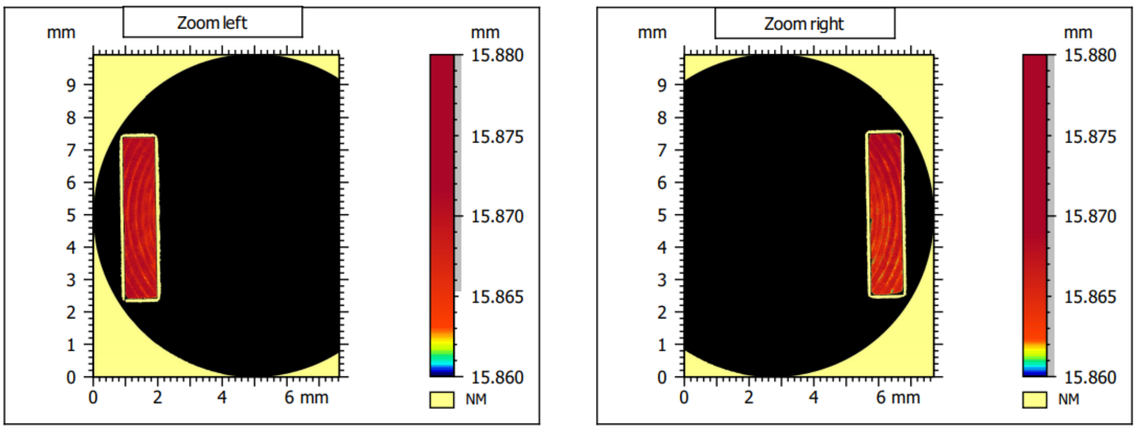

Figure 17 Wear volume analysis of the fixed specimen: zoom on the slider

The third step was aimed at computing the volume of the entire slider. For this purpose, an operator called "volume of peaks and holes" was used.

This operator computes the volumes of material above and below a reference plane: the sum of all the volumes above it is named “volume of the peaks” V_p, while the sum of those below it is named “volume of the holes” V_h (Figure 18).

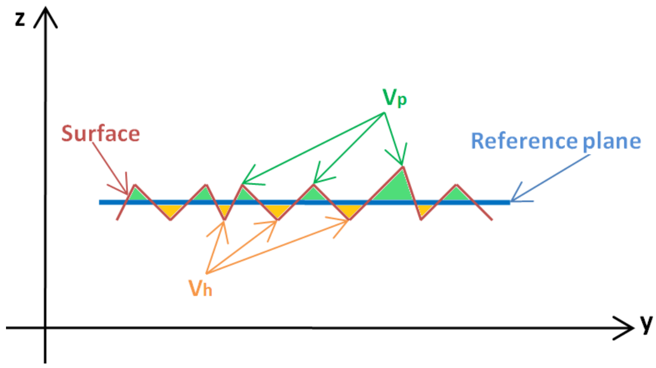

Figure 18 Volume of peaks and holes

In particular, after selecting an area, this operator takes as reference plane for the volume computation a mean plane calculated by extrapolation from the points outside the outline.

Figure 19a shows that the lower blue surface is automatically chosen as reference plane, when only the contact area (i.e. the slider) is selected. Since the slider was the only body above the plane, its volume was equal to that of the “peaks”; while the "holes" volume was equal to zero, since there was nothing underneath the reference plane.

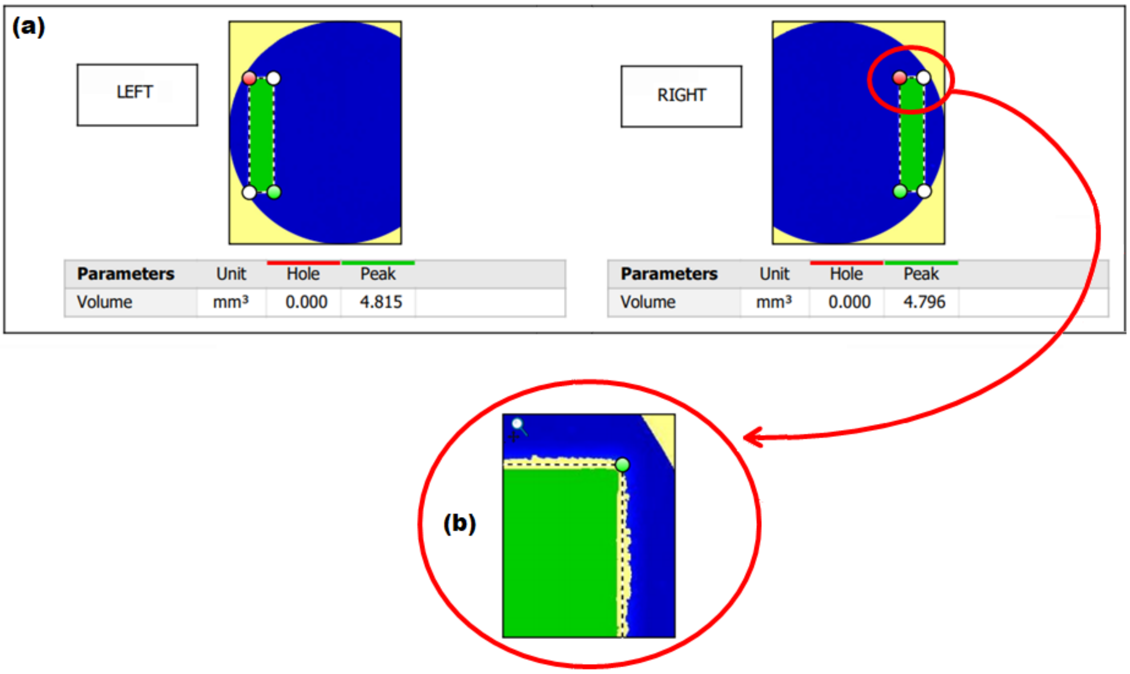

Figure 19 Wear volume analysis of the fixed specimen: a) volume calculation of the sliders; b) accurate selection of the contact area

As a consequence, an accurate area selection is obviously of the utmost importance (Figure 19b), since the measurement error would be significant if part of the slider volume is not considered.

Once the volumes of the unworn and worn sliders were obtained, the whole worn volume lost from the fixed specimen $V_{loss,fix}$ was calculated as the difference between the volume of the two sliders in the unworn condition $(V_{left}+V_{right})^{U,fix}$ and that in the worn condition $(V_{left}+V_{right})^{W,fix}$:

$$V_{loss,fix}= (V_{left}+ V_{right})^{U,fix} - (V_{left}+ V_{right})^{W,fix} \qquad (4)$$

Mobile specimen.

A slightly different approach was used in this case. Since the mobile specimen does not have sliders but the contact took place on the wider upper surface, also the volume of the holes was considered when using the "volume of peaks and holes" operator, taking as reference the mean plane within the sample surface.

Thus, the wear volume of the mobile specimen was estimated by measurements of peak and hole volumes in the contact area both in unworn and in worn conditions (Figure 20).

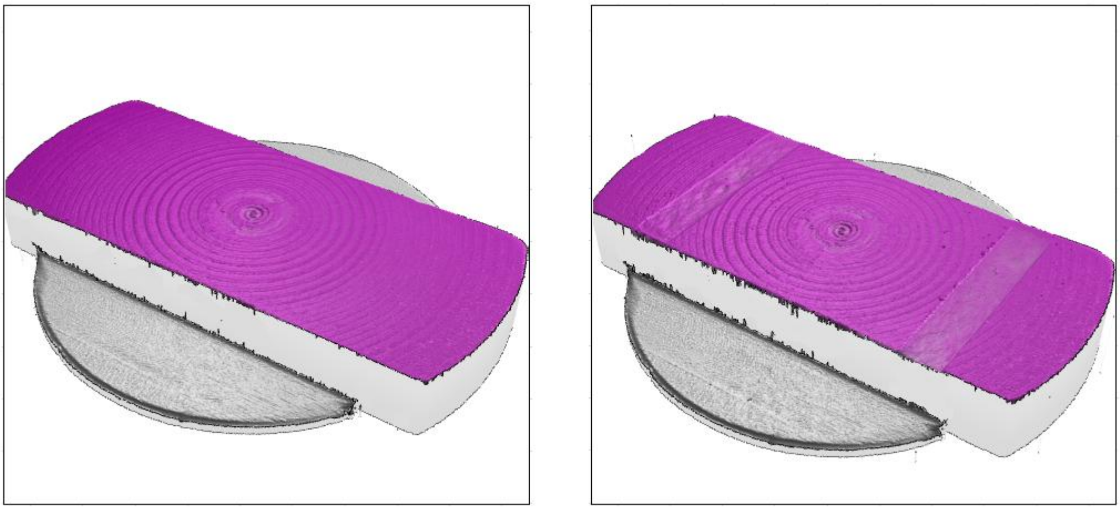

(a) (b)

Figure 20 3D view of a mobile specimen surface: unworn (a); worn (b)

A worn specimen is considered as an example for the illustration of the followed main steps; as for the fixed specimen, the procedure was performed in the same way for both the unworn and the worn contact surface.

The first step was aimed at obtaining the flat reference plane: a smooth macroscopic form was removed from the upper surface excluding the contact area; it was then levelled and the tilting was removed (Figure 21).

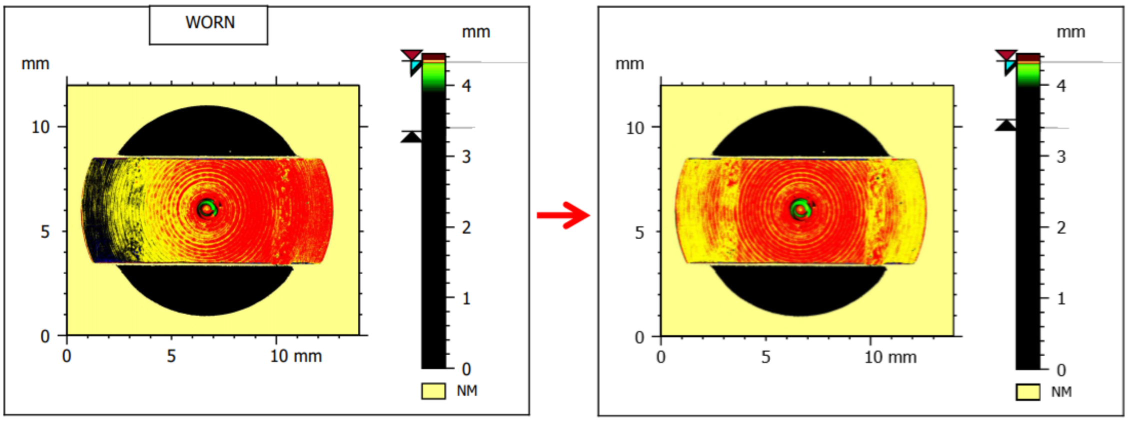

Figure 21 Wear volume analysis of the mobile specimen: remove form and level

Then, the lower background was excluded from the calculations (Figure 22).

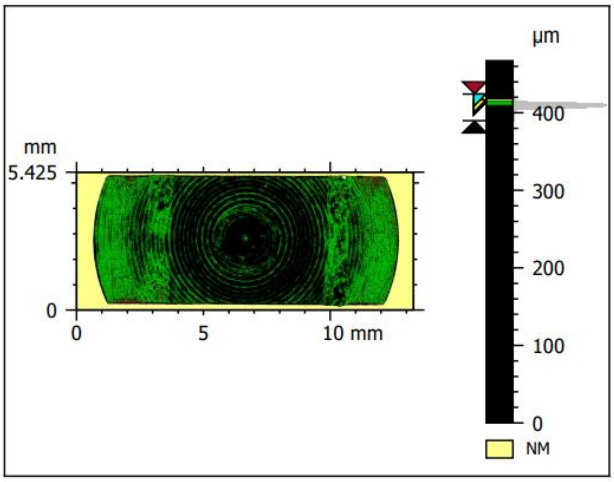

Figure 22 Wear volume analysis of the mobile specimen: zoom on the upper surface

The operator "volume of peaks and holes" was then used for the volume calculations. The reference plane was the mean plane within the sample surface obtained by extrapolation from the overall unworn points outside the selected contact area. The volumes of peaks and holes were evaluated in the worn area of the specimen as shown in Figure 23.

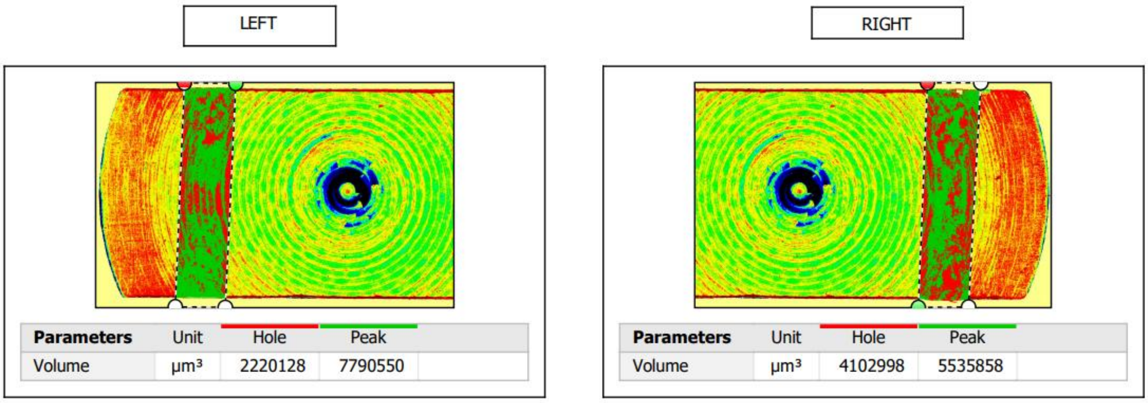

Figure 23 Wear volume analysis of the mobile specimen: volume calculation of peaks and holes

With regards to the specimen in unworn condition (before the wear process), the volume of peaks and holes was calculated in the corresponding area in which the wear scar would take place.

Once the volumes of peaks V_p and holes V_h in the contact area were obtained both in worn and in unworn condition, the whole worn volume lost from the mobile specimen $V_{loss,mob}$ was computed as[36]:

$$V_{loss,mob} = (V_{p,U} - V_{p,W}) + (V_{h,W} - V_{h,U}) \quad (5)$$

If the peak volume decreased and the hole volume increased with respect to the unworn condition, then there was a loss of material from the mobile specimen.

Finally, the total volume loss from the pair of specimens V_{loss} during the fretting wear mechanism was obtained as:

$$V_{loss} = V_{loss,fix} + V_{loss,mob} \quad (6)$$

4.3. **Worn area estimation**

Worn areas of contact were carefully detected on the optical topographic measurement of each specimen after the wear process using the software MountainsMap.

In Figure 24 an example of worn area measurement for specimens with nominal contact area of 10 mm^2 is shown.

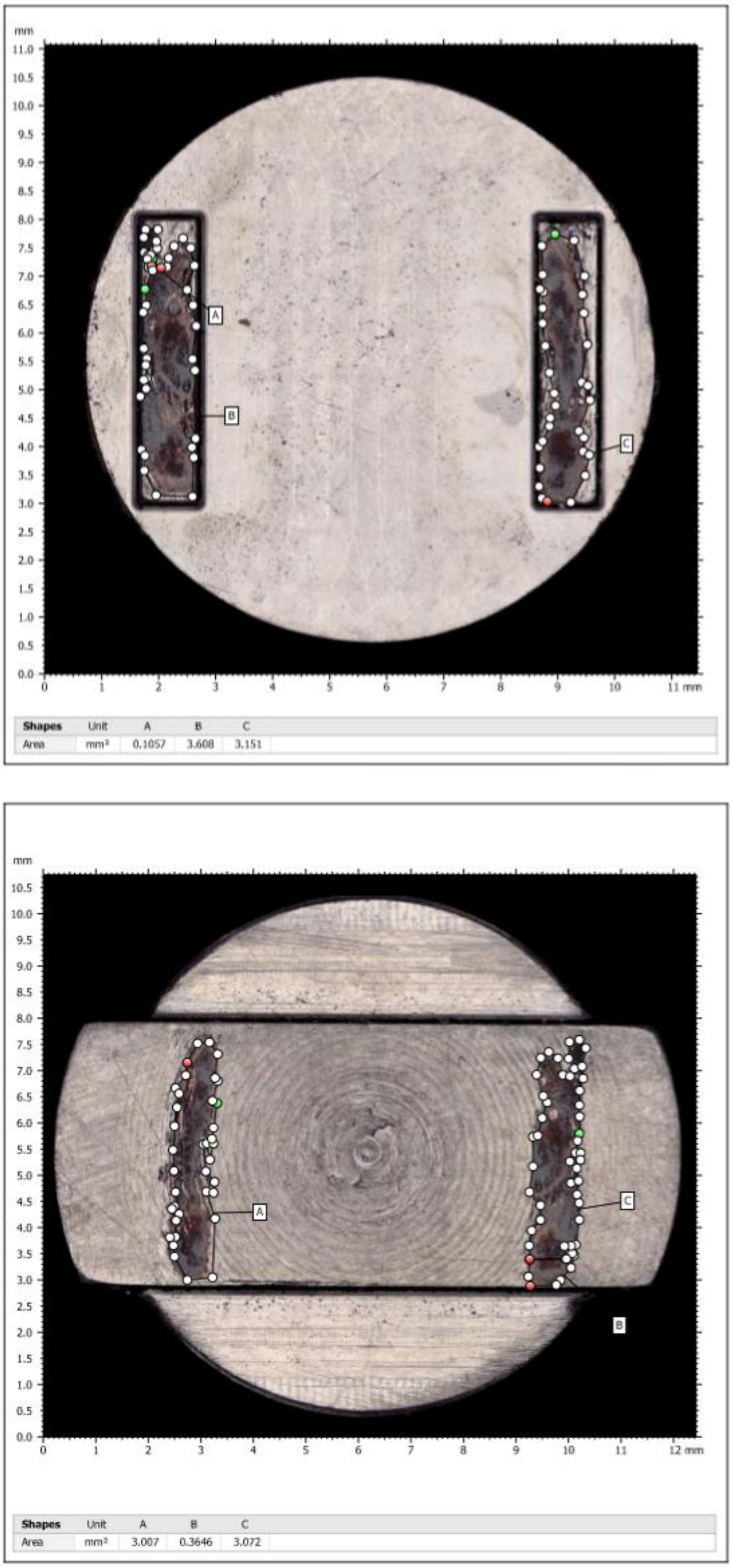

Figure 24 Example of worn area detection

Chapter 5

5. Experimental campaign

The experiments carried out for this study were performed on the test rig designed at LAQ AERMEC laboratory of Politecnico di Torino in 2010 and described in the Chapter 3.

A series of fretting tests was conducted at room temperature using different couples of specimens, made of stainless steel (SS304). All tests were performed with an excitation frequency of 175Hz, which is the optimal one for the test rig.

Before each test an air gun was used to remove eventual dirt and dust from specimens' contact interfaces, which were scanned using the Alicona – InfiniteFocus optical 3D measurement system; after each experiment, the specimens were removed from the test rig and optical microscope images of their surfaces were captured again for the subsequent wear analysis, as explained in the Paragraphs 4.2 and 4.3.

The aim of the experimental campaign is to identify the behaviour of the friction contact parameters resulting from different operating conditions: normal loads, sliding amplitudes and nominal areas of contact, which were varied according to a pre-established experimental plan. The latter and the results are discussed in the following paragraphs.

5.1. **Experimental Plan**

Couples of specimens with three different areas of contact have been considered, in order to evaluate how the friction contact parameters are influenced by the extension of the "nominal" contact surface and how they change under the same loading conditions and relative displacements (Figure 25). The nominal contact areas considered are: 5 mm^2 (Figure 25a-d), 10 mm^2 (Figure 25b-e), and 40 mm^2 (Figure 25c-e).

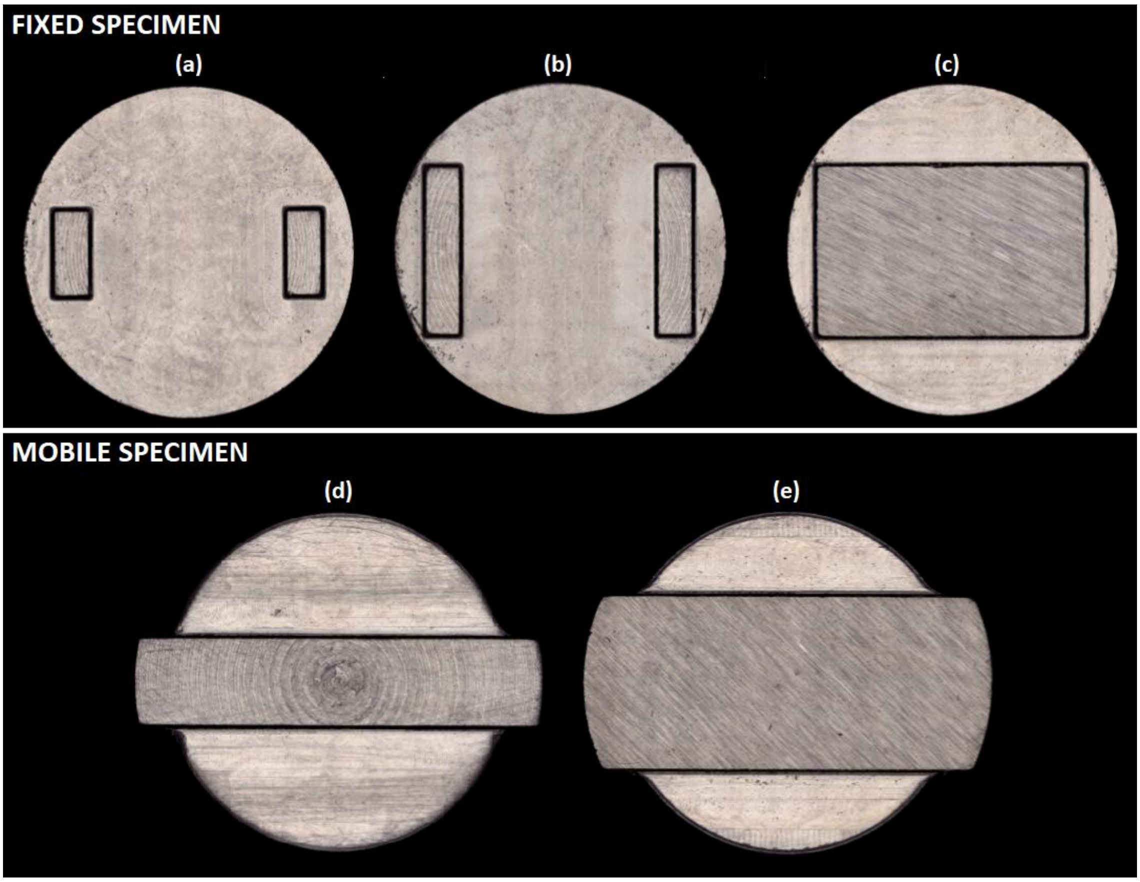

Figure 25 Fixed specimen: 5 mm^2(a), 10 mm^2(b), 40 mm^2(c); Mobile specimen: 5 mm^2(d), 10 mm^2 and 40 mm^2(e)

With regards to the fixed specimen, contact areas of 5 mm^2 and 10 mm^2 are obtained by means of two sliders, while in the case of 40 mm^2 contact area there is a single slider.

Three matrices of experiments were designed (one for each nominal contact area chosen). Each matrix is characterized by 3 different values of normal load and relative displacement (Figure 26).

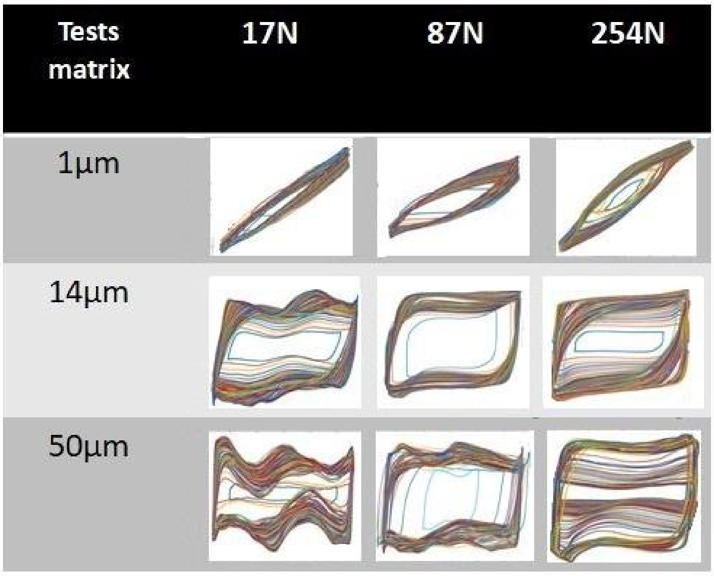

Figure 26 Tests matrix

The normal loads applied were 17N, 87N and 254N; while the displacements imposed were 1µm, 14µm and 50µm, considering in such a way the three different regimes of fretting (stick regime, mixed stick-slip regime and gross slip regime respectively).

The tests were performed for 2,5 hours. Nevertheless, long-term tests (until 12 hours) were also run to verify that, after a certain running-in period, the contact parameters remained constant in time. In fact, the effects of wear over time on the evolution of the frictional contact parameters have to be investigated since turbomachinery run into service for much longer times (e.g. an aero engine could work for 10 consecutive hours during a flight).

5.2. **Results and interpretation**

In this section, trends of the friction contact parameters are evaluated against time, worn area of contact, normal load and sliding distance, in order to investigate their effect on the friction coefficient and tangential contact stiffness.

5.2.1. Friction contact parameters over time

For all the tests an analysis of the hysteresis loops evolution over time was carried out in order to investigate the effects of wear on the friction contact parameters. Long-term tests have been run to ensure that, after a certain running-in period, the contact parameters remained constant in time.

In Figure 27 the evolution of contact parameters over time is shown as an example for one of the tests (the trend is in general the same for all other tests). This test was run at 175 Hz for 5 hours with a constant normal load (87 N) and a constant relative displacement (14 μm).

As can be seen from Figure 27, both friction coefficient and contact stiffness are strongly influenced by the running-time.

The friction coefficient (Figure 27b) was calculated in two ways: as the ratio between the friction limit and the normal load (blue trend) and by means of the energy dissipated (orange trend), as explained in the Paragraph 4.1. Whereas, the tangential contact stiffness (Figure 27c) was estimated from the left side of the loop k_{tL} (blue trend) and the right one k_{tR} (orange trend).

At the beginning of the test there is a substantial evolution of the contact parameters, which is discussed in the next paragraphs.

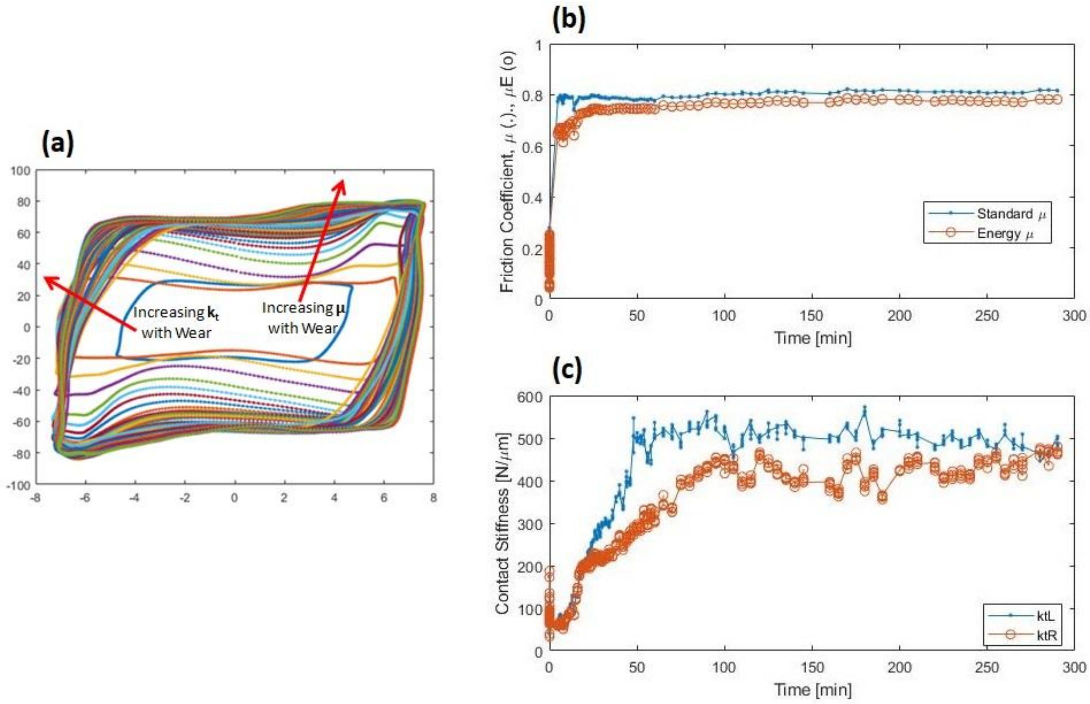

Figure 27 Effects of wear for Test 14: normal load 87N, relative displacement 14µm, nominal area 10mm^2 a) Hysteresis loop evolution over time; b) friction coefficient over time c) Tangential contact stiffness over time

Friction coefficient

Figure 27a shows how the hysteresis loop changed during the test run as time went on. It is evident that the macroslip portion of the hysteresis loop shifts upwards, thus increasing the friction limit T= μN at which the contact starts to slide; this shift indicates an increase in the friction coefficient μ, since the normal load N was maintained at a constant value during the whole test.

In Figure 27b the trend of the friction coefficient over time is shown. It rapidly increases at the beginning of the fretting process; for this reason, the trend is shown in log scale with respect to time in Figure 28.

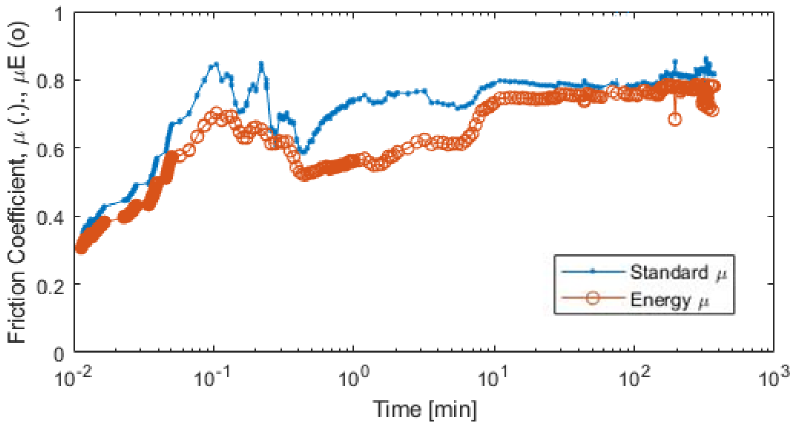

Figure 28 Friction coefficient in log scale with respect to time

The friction coefficient increases within approximately 5 seconds (less than 1000 fretting cycles) from the beginning of the test, exhibiting a local maximum. After this "running-in period", it decreases and then it still increases in time with a lower rate, reaching a steady state value. The same trends have been obtained in other previous studies using similar rigs [3].

The physical reason of the rapid increase of the friction coefficient in the beginning of the test could be related to the removal of the initial layers (absorbed gas, oxide) present on the contact surfaces [3], [37]. In fact, the existence of these layers do not allow the full adhesion between contact interfaces. After the first thousands of fretting cycles, such layers are removed resulting in a metal-to-metal and/or metal-to-wear particles contact; this leads to an increase of the adhesive and ploughing components of the friction coefficient. Finally, the friction coefficient reaches a steady state value when surface layers are completely removed and a balance is achieved between generation and ejection of wear debris from the contact [38].

Tangential contact stiffness

With regards to the tangential contact stiffness, the slope of the stick portion of the loops increases as can be seen from the hysteresis loop evolution over time (Figure 27a).

Values of tangential contact stiffness were estimated from both sides of the loops (k_{tL} and k_{tR}), showing a slightly different trend. The reasons for this behaviour are still not entirely clear, and further tests will be conducted in the future to investigate it more in detail. The difference could be due to the physics of contact which behaves asymmetrically with regards to the sliding direction or it is dueto the mechanical behaviour of the friction rig.

A gradual increase in the tangential contact stiffness occurs during the "running-in period" (Figure 27c); then, both k_{tL} and k_{tR} converge towards constant values respectively after about 50 minutes (525.000 cycles) and 100 minutes (1.050.000 cycles) from the test's start.

This increase in the contact stiffness during the running-in period might be due to an increased conformity of the contact interfaces, which leads to a larger amount of asperities in contact, thus contributing to the increase in the contact stiffness [3]; then, the steady state is reached when a full interaction between the contacting interfaces is attained.

To give an explanation of this interpretation, it is important to clarify that no real ("engineering") surface is ideally smooth. The surface is characterised by irregularities (protuberances or asperities) left by any machining process used to finish it.

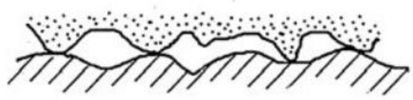

Figure 29 Schematics of an engineering interface

Consequently, when surfaces get in touch, the real area of contact is smaller than the nominal (or apparent) one [39]; true contact occurs only at the crests of higher surface asperities (Figure 29). As explained in Paragraph 2.3, the physical origin of contact stiffness is attributed to the elastic deformation of these asperities coming into contact.

Thus, the rapid increase of the tangential contact stiffness with increasing fretting cycles during the running-in period suggests that a larger amount of asperities gets in contact, increasing the conformity of the contact interfaces. The more the asperities in contact, the higher the elastic deformations contributing the stiffening of the contact interfaces. When the contact surface conditions stabilize, the contact stiffness reaches a steady state.

A detailed analysis of the worn area of contact was carried out to further investigate this wear dependence, and it is here hypothesized that the tangential contact stiffness might reach a steady state probably for the following two reasons:

1. The steady state in the tangential contact stiffness is reached when the worn area becomes equal to the “nominal area”, as shown in Figure 30, where the whole contact area is black due to a full oxidation. This would mean that the “full worn area of contact” is reached around 50 minutes, when the steady state in the contact stiffness is reached.

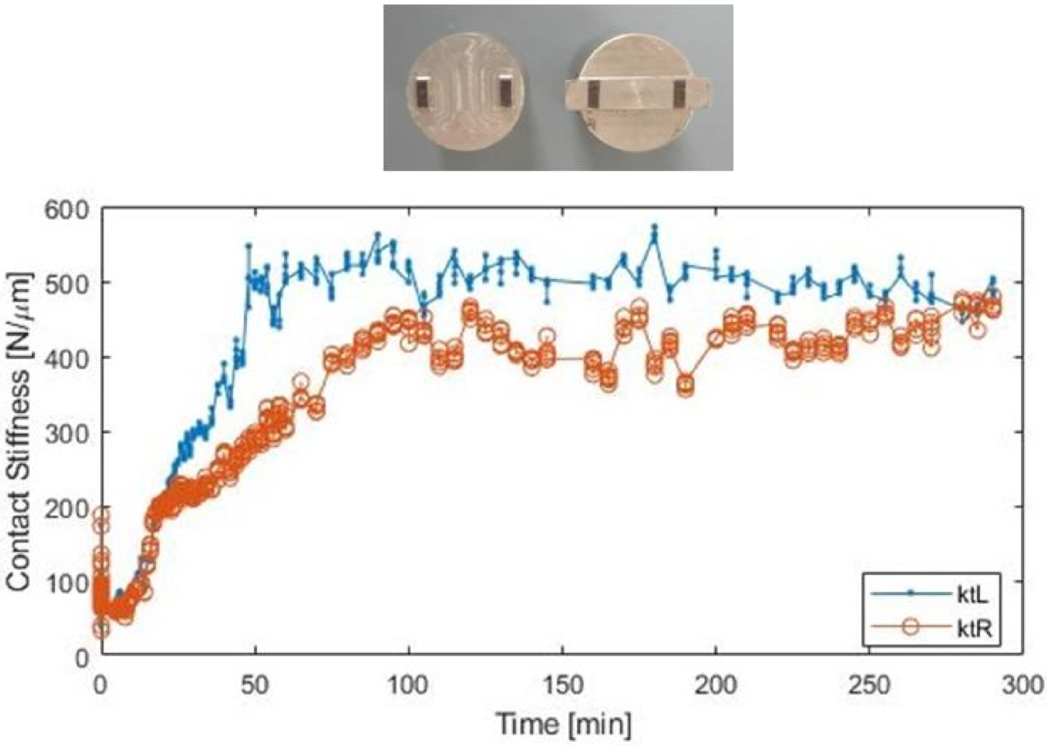

Figure 30 Tangential contact stiffness over time and picture of worn areas (Test 14: normal load 87N, relative displacement 14µm, nominal area 5mm^2). Here the steady state is probably reached when the worn area extends over the whole nominal area.

2. The steady state in the tangential contact stiffness is reached when the worn area stops to grow even if energy is still being dissipated, as shown in Figure 31. This "locking" of the worn area (which stops to grow) probably occurs for tests conducted with specimens marked by a particular superficial waviness that leads to uneven wear distributions. In particular, the worn area "locks" only for tests in mixed stick-slip regime conditions (relative displacement of 14 µm) because probably there is not enough sliding to have full wear and consequently the worn area is not capable to extend over the whole contact. This "locking" of the worn area indicates the following: the fact that the contact stiffness reaches the steady state cannot be a clear

indication that the worn area has fully spread out over the whole nominal area, since a “locking” might have also been occurred. Therefore, the trend of the contact stiffness cannot be used to get insights on the “distribution” of the worn area, but can only give information on the “steady state” in the evolution of the worn area of contact (that can be either due to “locking” or to reaching of full nominal area).

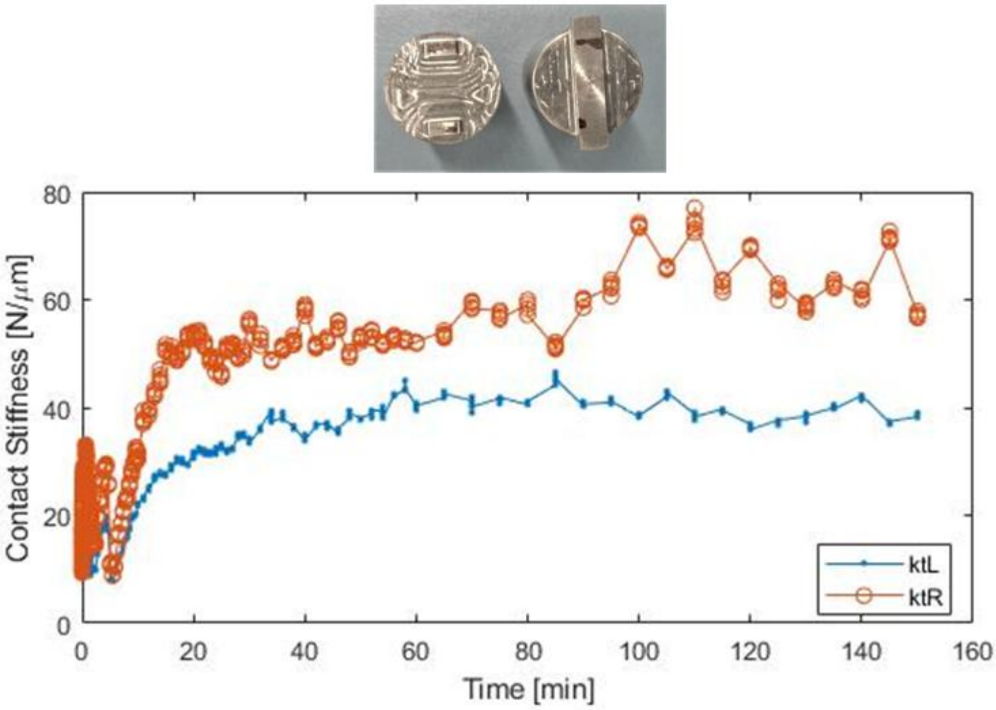

Figure 31 Tangential contact stiffness over time and picture of worn areas (Test 25: normal load 87N, relative displacement 14μm, nominal area 5mm^2). Here the steady state is probably reached when the worn area “locks” and stops to increase, probably due to an uneven waviness of the contact.

This dependency of the tangential contact stiffness on the worn area of contact indicates that the contact stiffness probably does not depend only on the number of asperities in contact, but also on the increased interaction between wear scars with fretting cycles: peaks and holes become conforming and lock the surfaces together, adding elastic resistance to the tangential relative motion during the stick phase, thus increasing k_t.

Thus, the contact stiffness increases with the worn area increasing. The steady state is reached when the worn area does not increase anymore and the highest compliance between the two surfaces is attained, as suggested also from the results of similar friction rigs [3].

In conclusion, this phenomenon suggests a novel result: in fretting wear conditions, the tangential contact stiffness converges towards a constant value probably when the maximum conformity due to wear is attained over the whole nominal areas of contact. In other words, k_t is worn area dependent. This dependency is further investigated with the following detailed analysis.

In general, a linear trend is obtained when the steady state value[1] of the tangential contact stiffness is plotted versus the worn area of contact for tests carried out in the same operating conditions (normal load and relative displacement) and with the same nominal area of contact. Figure 32 shows the trend obtained from tests performed using specimens with 10 mm^2 of nominal contact area under normal load and relative displacement of respectively 87 N and 14 μm.

[1] Since the measured contact stiffness shows a certain variability around the steady state value, box plots are used. On each box, the central mark indicates the median, and the bottom and top edges of the box indicate the 25th and 75th percentiles, respectively. The whiskers extend to the most extreme data points not considered outliers, and the outliers are plotted individually using the '+' symbol.

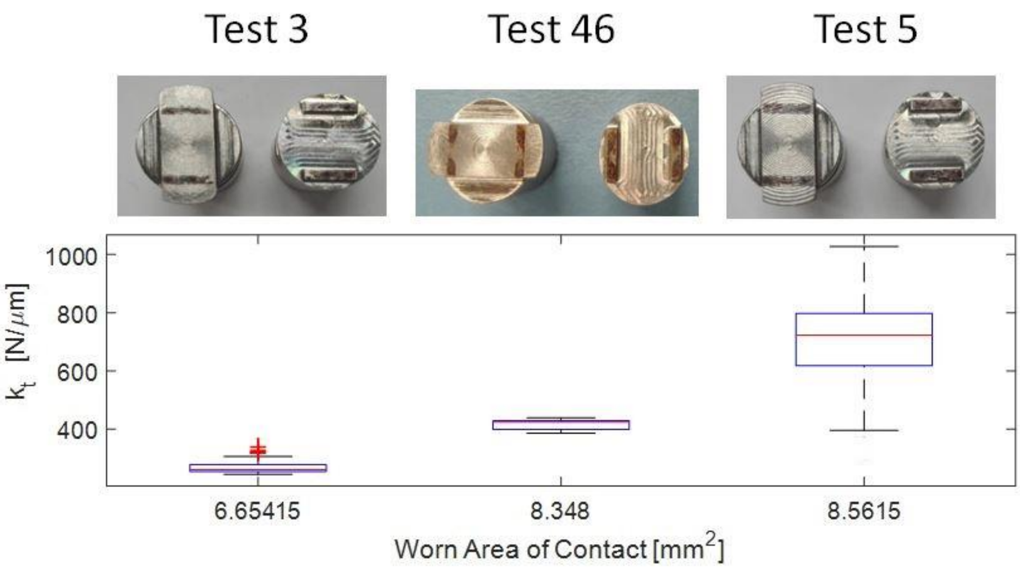

Figure 32 Tangential contact stiffness vs worn area of contact (normal load 87N, relative displacement 14µm, nominal area 10mm2)

This linear dependency of the contact stiffness on the worn area of contact confirms the physical interpretation given before: with a larger worn area of contact, more asperities and/or wear scars interact, resulting in a higher number of elastic deformations; as a consequence, a higher final value of contact stiffness is reached.

This original result suggests that the "worn" area of contact should be considered for the normalization of the contact stiffness rather than the nominal one, as is currently done in nonlinear dynamics simulations [40].

Another phenomenon is observed plotting the steady state values of tangential contact stiffness versus worn area of contact for tests carried out in the same operating conditions (normal load and relative displacement) but using specimens featured by a different nominal area of contact (5 mm^2, 10 mm^2 and 40 mm^2).

Two trends are illustrated by way of example: they are obtained from tests performed with normal load and relative displacement of respectively 87 N and 14 µm (for the first trend, Figure 33) and 254 N and 14 µm (for the second one, Figure 34).

In both cases, the tangential contact stiffness for tests with nominal area of 40 mm^2 (Test 32 and Test 31) is lower even if the worn area is larger. This decrease in the contact stiffness for the 40 mm^2 tests is probably due to the fact that in both contact surfaces the individual worn zones are spread out over the whole contact surface. If this is the reason, then this result indicates that the tangential contact stiffness is strongly dependent on the distribution as well as the number and the size of the individual worn regions of contact. If the worn zones are spread over a large nominal area, the measured contact stiffness is lower.

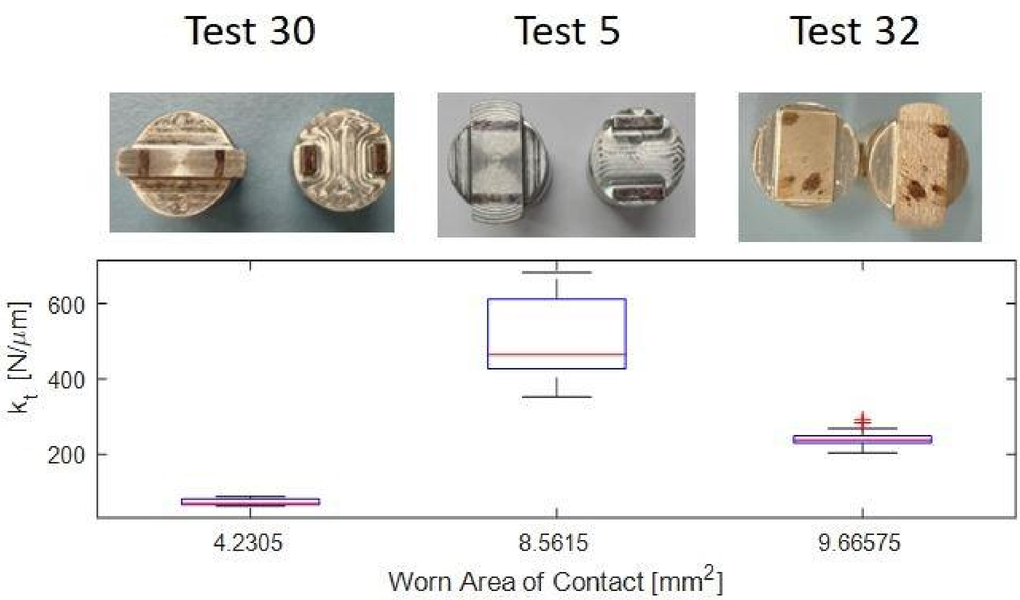

Figure 33 Tangential contact stiffness vs worn area of contact (normal load 87N, relative displacement 14µm, nominal area of 5 mm2, 10mm2 and 40mm2)

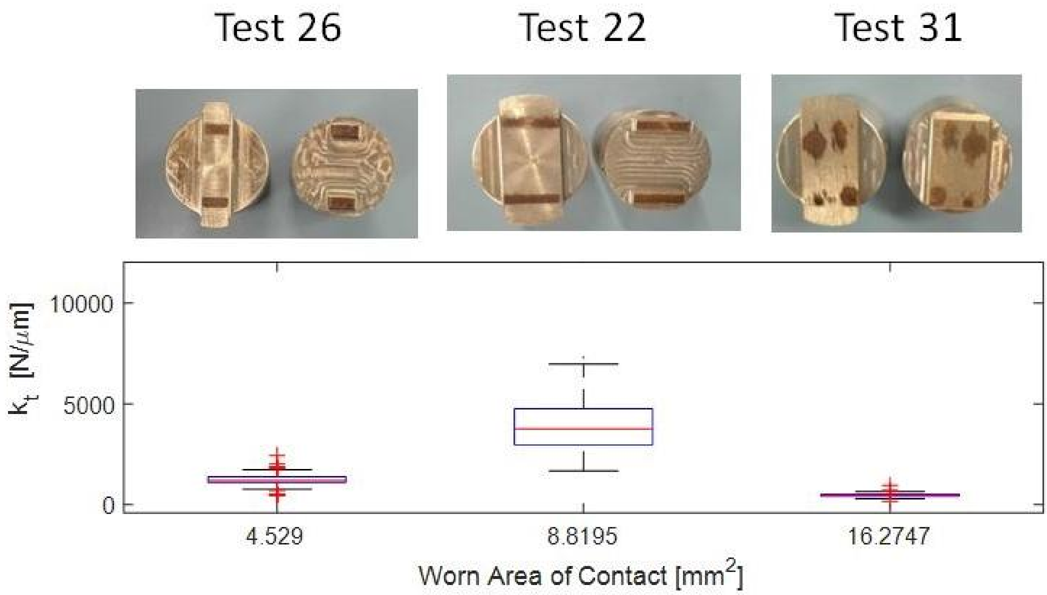

Figure 34 Tangential contact stiffness vs worn area of contact (normal load 254N, relative displacement 14µm, nominal area of 5 mm2, 10mm2 and 40mm2)

To confirm this hypothesis, Figure 35 shows that when a full worn area of contact is reached, the trend is again linear, with the 40 mm^2 test showing the larger values in the contact stiffness.

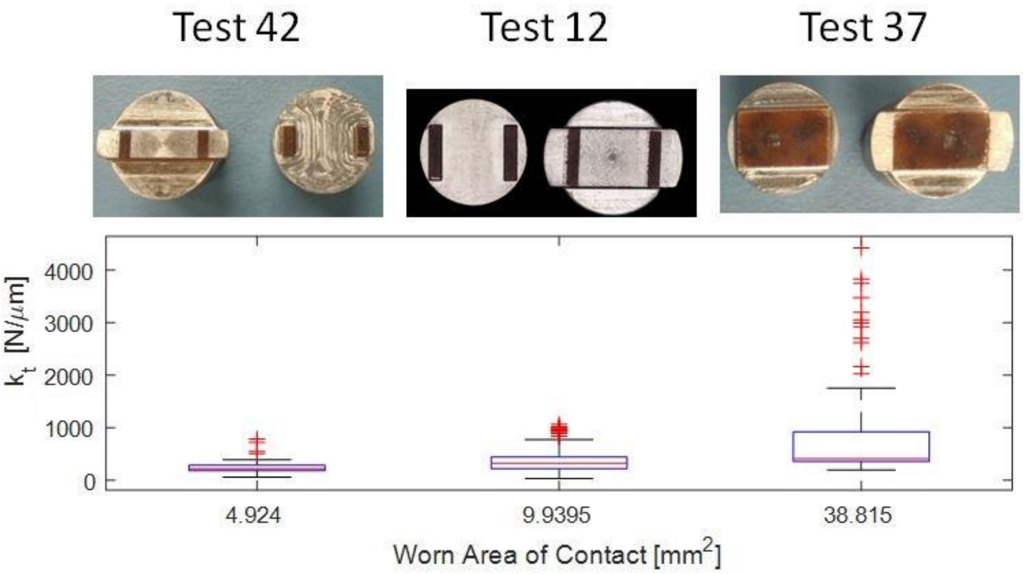

Figure 35 Tangential contact stiffness vs worn area of contact (normal load 254N, relative displacement 50µm, nominal area of 5 mm2, 10mm2 and 40mm2)

It can be seen that the trend is again linear, as in the case of Figure 32. It could be concluded that the tangential contact stiffness depends on the configuration of the worn area of contact, which in this case covers the whole contact, while in the cases of Figure 33 and Figure 34 was scattered over the whole interface.

Finally, a further analysis was conducted to investigate how the worn area evolves over time, and it was found that the amount of worn area depends on the energy dissipated, as could be expected intuitively: the larger the worn area, the more the energy dissipated on the contact surfaces.

This dependency is confirmed plotting the worn areas' dimensions over the amount of energy dissipated to reach the steady state values of contact stiffness for tests under the same operating conditions but with different nominal areas (in Figure 36 tests performed with normal load and relative displacement of respectively 254 N and 50 µm are considered by way of an example).

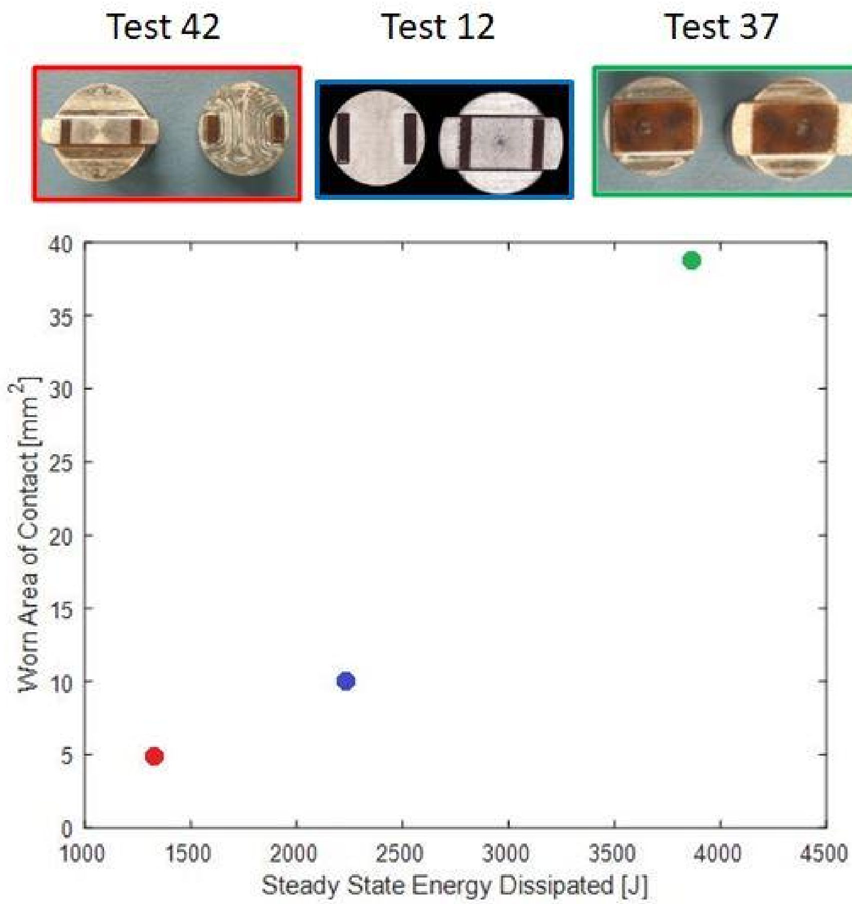

Figure 36 Worn area of contact vs steady state energy dissipated (normal load 254N, relative displacement 50µm, nominal area of 5 mm2, 10mm2 and 40mm2)

The analyses conducted so far, regarded only tests performed at 14 µm and 50 µm, where there was enough energy dissipated for the generation of a worn area of contact. When the tests are performed at 1 µm, there is no energy dissipated and consequently no worn area of contact appears. The behaviour of such tests is discussed in the following paragraph.

5.2.2. Tangential contact stiffness evolution in stick tests

For tests in stick regime conditions (marked by very limited surface damage related to corrosion and wear) it is also observed that the tangential contact stiffness increases even if there is no worn area, as shown in Figure 37. In this case, it is hypothesised that the increase in the contact stiffness is not due to an increased conformity of the contact interfaces due to a worn area, but it is due to a plasticity hardening of the asperities undergoing continuous loading and unloading cycles. In fact, during the stick test the dissipated energy and the sliding distance are so small that no worn area occurs, but the asperities are continuously loaded and unloaded: this makes them harder due to a plasticity hardening, which leads to an increase in the tangential contact stiffness.

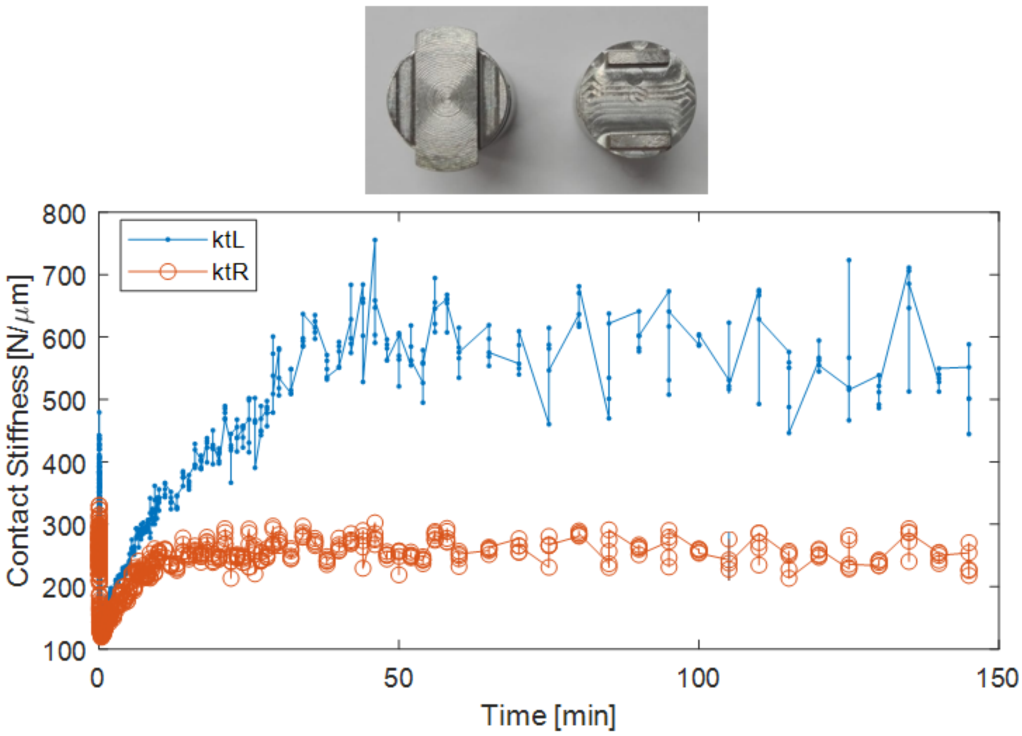

Figure 37 Tangential contact stiffness over time and picture of worn areas (Test 10: normal load 87N, relative displacement 1μm, nominal area 10mm2)

Furthermore, it is also observed that for few stick regime tests using specimens with 40 mm^2 of nominal area, the tangential contact stiffness appears to reach the steady state only at the end of the experiment (an example is shown in Figure 38) and not after only 20 minutes as in Figure 37. This longer time needed for reaching the steady state might be due to a larger dispersion of the real contact regions over the larger nominal area.

Concluding, this Section has shown that tangential contact stiffness experience a running-in increase before reaching a steady state. In the case of gross slip and mixed stick-slip tests it is hypothesized that the increase is due to an increase in the worn area of contact. In the case of stick tests, it is hypothesized that the increase is due to a plasticity hardening of the contacting asperities.

In the next paragraph, the effect of the normal load is investigated.

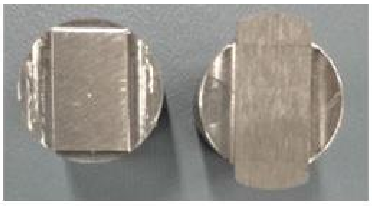

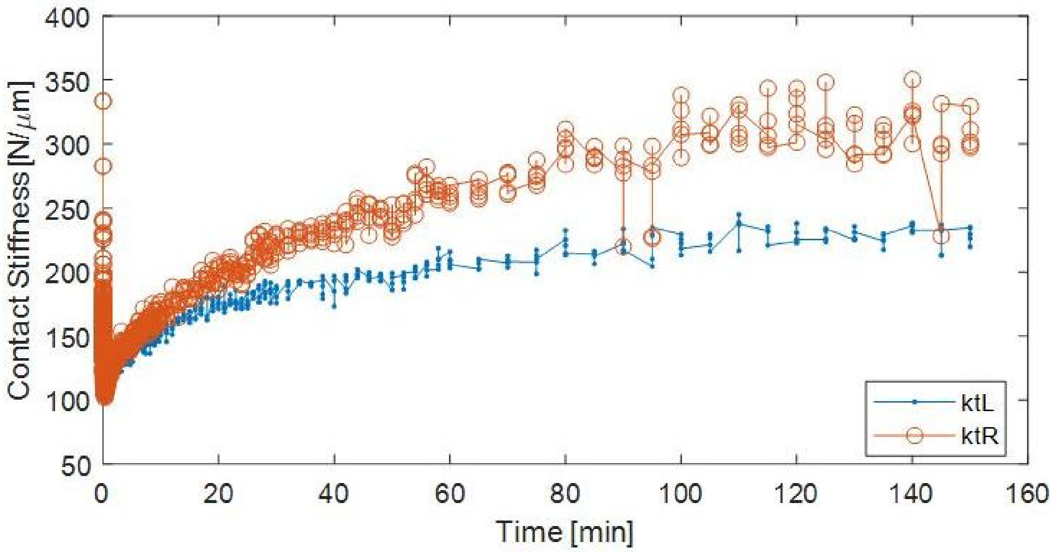

Figure 38 Tangential contact stiffness over time and picture of worn areas (Test 36: normal load 87N, relative displacement 1µm, nominal area 40mm2)

5.2.3. Normal load influence

The influence of the normal load on the friction coefficient and the tangential contact stiffness is investigated by comparing tests performed at varying normal loads and same sliding distance and specimens' nominal area of contact. In particular, the steady state values of the two contact parameters are considered for each test. One hysteresis loop for each test is shown in Figure 39.

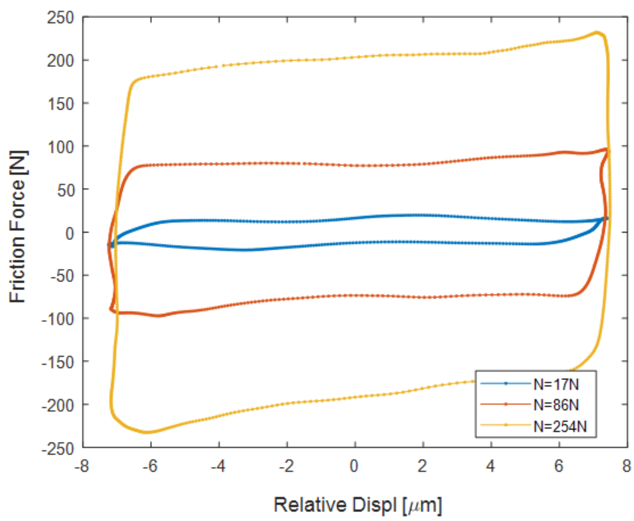

Figure 39 Hysteresis loops for different normal loads and the same sliding distance

Friction coefficient

Three tests conducted for specimens with a nominal area of contact of 5 mm^2 at 14 μm of sliding distance are here discussed by way of example (as the trends are the same for all the experiment's combinations).

As shown in Figure 39, the higher the normal load, the higher the friction limit, at which the contact starts to slide. However, the friction coefficient remains almost constant (Figure 40).

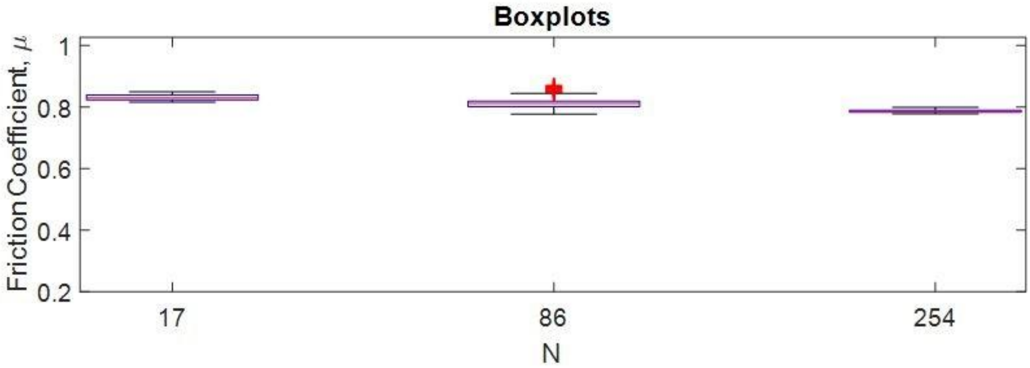

Figure 40 Friction coefficient vs normal load

These results confirm that for dynamic simulations just a single value for the friction coefficient is required in the case of normal load variations.

Tangential contact stiffness

With regards to the contact stiffness, in Figure 39 it is evident that the slope of the stick portion of the hysteresis loops increases from the blue loop to the yellow one. Figure 41 shows the contact stiffness versus the normal load. It is clear that the contact stiffness is strongly affected by the normal load, with a behaviour similar to the ones found in literature (see Figure 7 for comparisons).

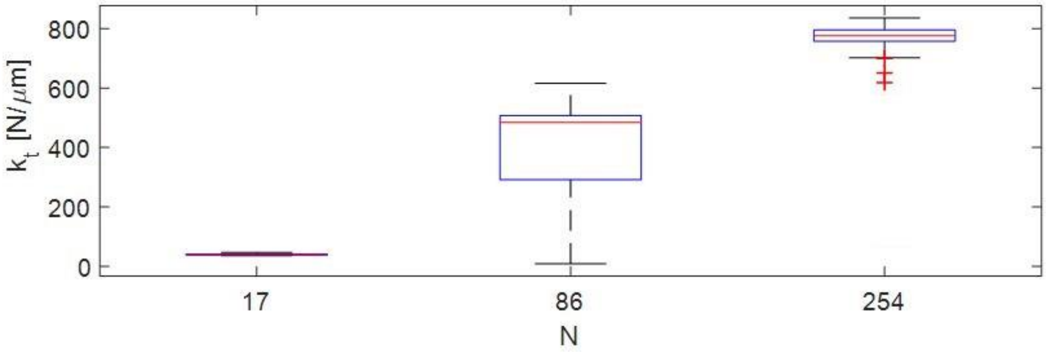

Figure 41 Tangential contact stiffness vs normal load

The contact stiffness for the test under 17 N is considerably lower than for the one under 86 N; the difference is less marked between the latter case and the one under 254 N. At light loads the contact stiffness is lower because only few asperities come into contact, and therefore the amount of elastic interactions that generate the contact stiffness is limited. As the load increases, more asperities come into contact rapidly, thus contributing to increases in the contact stiffness.

This result confirm that contact stiffness needs to be modelled in dynamics simulations as a function of the normal load.

5.2.4. Relative displacement influence

With the aim to investigate even the influence of the relative displacement on the friction contact parameters, several comparisons were made between experiments under the same normal load using specimens with equal nominal area. The steady state values of contact parameters are considered for each test. One hysteresis loop for each test is shown in Figure 42.

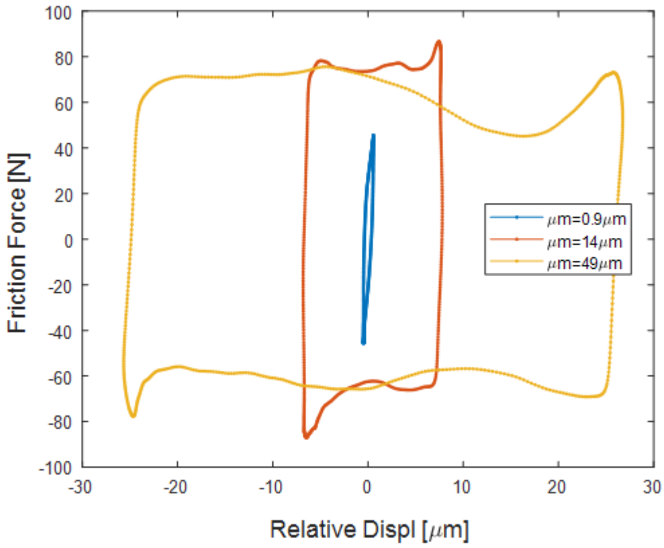

Figure 42 Hysteresis loops for different sliding distances and the same normal load

Friction coefficient

For the evaluation of effect of the sliding distance on the friction coefficient, tests with 1 μm of relative displacement are obviously not considered, since this condition corresponds to a pure stick fretting regime (there is no sliding).

Two mm^2 tests performed with specimens with a nominal area of contact of 10 mm^2 under 87 N of normal load are considered by way of example.

As shown in Figure 42, by increasing the relative displacement from 14 μm to 50 μm, the friction limit remains on average the same; since equal normal load was imposed during the tests, the friction coefficient remains almost constant (Figure 43).

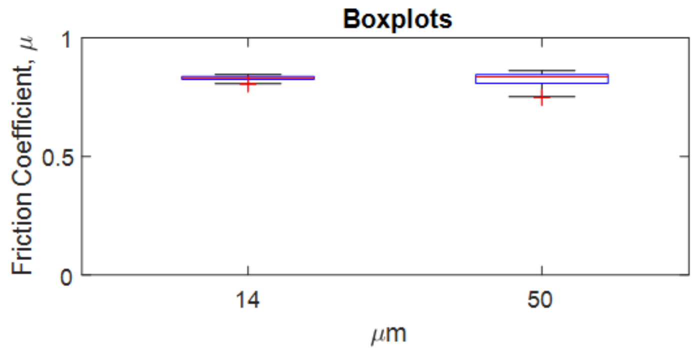

Figure 43 Friction coefficient vs relative displacement

Tangential contact stiffness

Figure 44 shows a clear decrease in the tangential contact stiffness with the sliding distance comparing 10 mm^2 tests under 87 N of constant normal load.

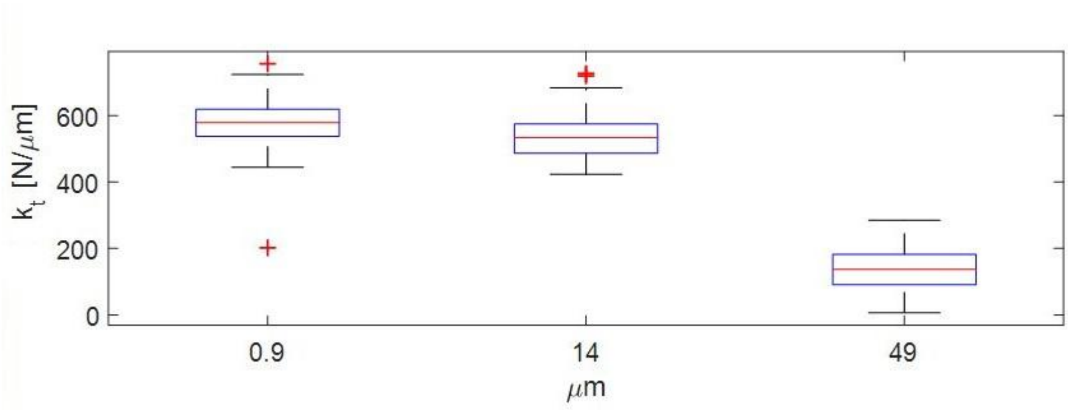

Figure 44 Tangential contact stiffness vs relative displacement

The decrease in the contact stiffness with sliding distance might be explained by the junction growth phenomenon described in [41]. Bowden and Tabor stated that when a load (normal or tangential) is applied on two contacting interfaces, the real area of contact between the asperities will increase in order to accomodate such load (i.e. a junction growth will appear). Hence, when a tangential load is applied, the real area of contact would slightly increase, thus leading to increases in the contact stiffness.

However, at larger sliding distances, the velocity would be so large that there would be not enough time for the junctions to grow within the hysteresis cycle, hence leading to a reduced contact stiffness.

To further investigate this velocity dependence, a test was conducted with a fixed normal load and a wide range of sliding distances by using the same couple of specimens. The hysteresis loops are shown in Figure 45.

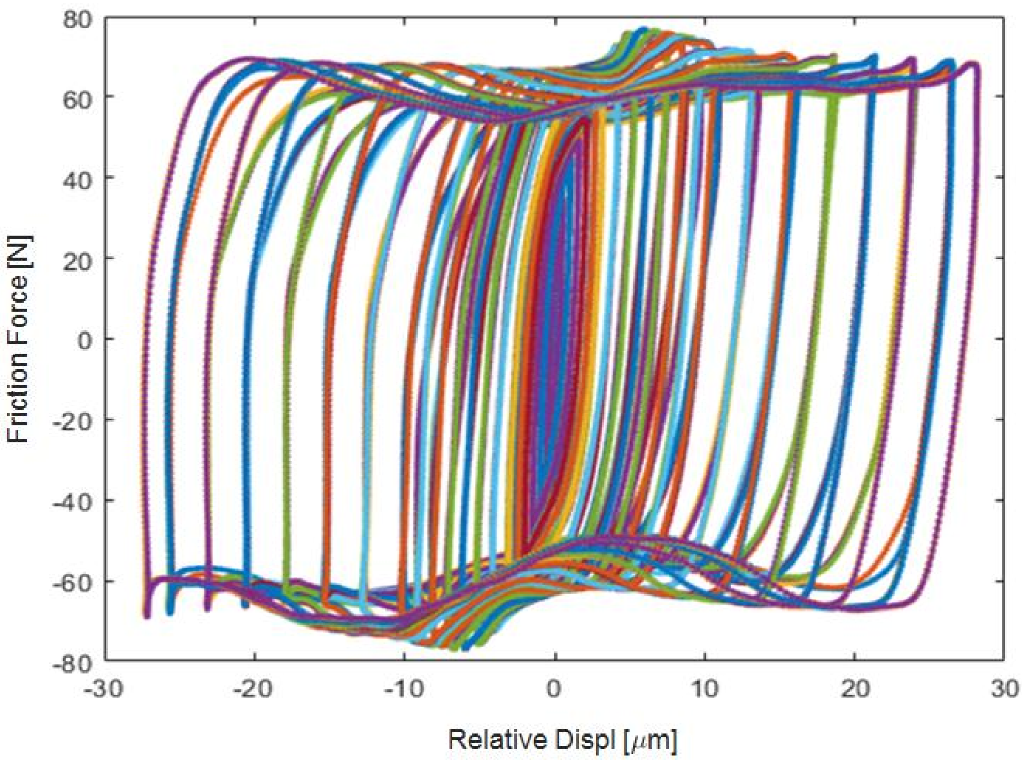

Figure 45 Hysteresis loops for different sliding distances

After reaching full worn area of contact to ensure a high compliance between the contact surfaces, the relative displacement was gradually decreased from 50 μm to 0 μm and then again increased to 50 μm, with a normal load of 87 N fixed during the whole test.

Figure 46 shows the trends of the ratio T/N, the slip displacement and the tangential contact stiffness over time.

The results confirm the trends obtained above:

- The friction coefficient remains almost constant. When the relative displacement is so low to have stick regime conditions, the ratio T/N is no more representative of the friction coefficient.
- The contact stiffness increases for decreasing sliding amplitudes, and vice versa.

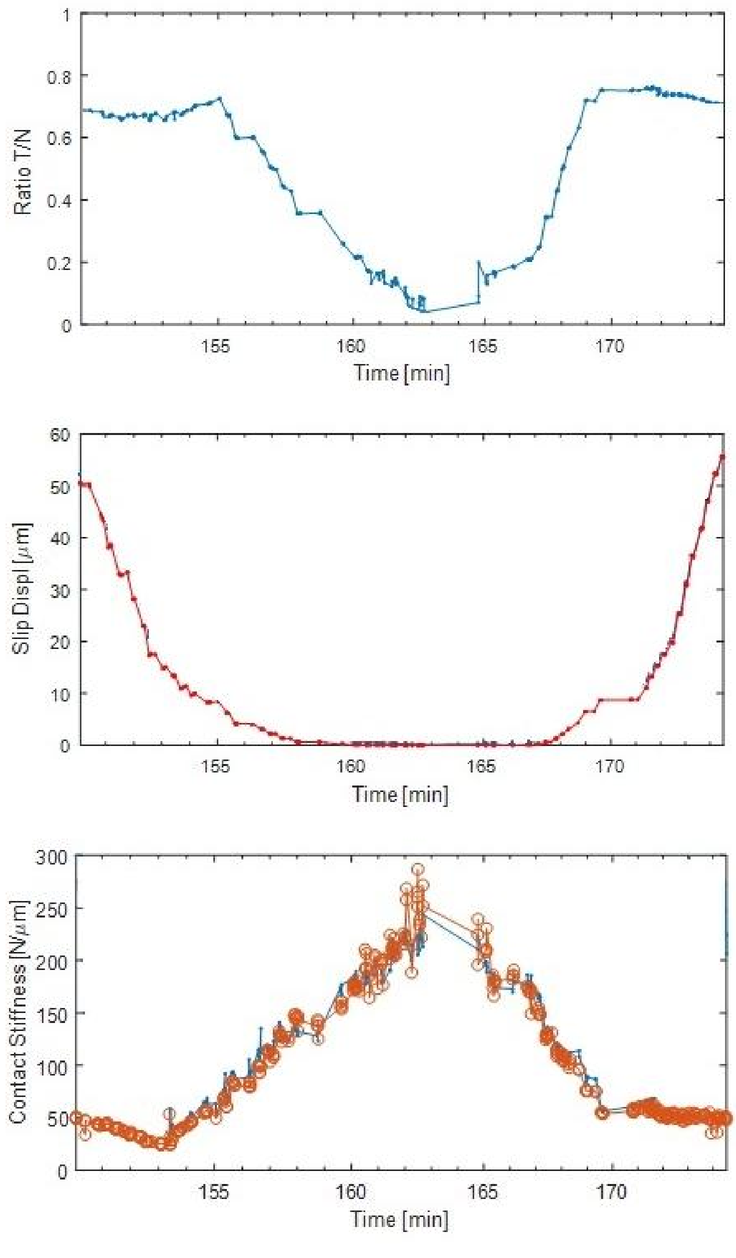

Figure 46 Full sliding test: a) Ratio T/N over time, b) Slip displacement over time, c) Tangential contact stiffness over time

5.2.5. Wear volume analysis

A particular procedure was performed to estimate the volume of material loss by the surfaces during the fretting process for each test. The values obtained are showed below for one test by way of an example. For this experiment a couple of specimens with nominal area of 10 mm^2 were used; it was carried out under 254 N of normal load and with 14 µm of sliding distance.

Fixed specimen

As explained in detail in Chapter 4, the wear volume of the fixed specimen was calculated as the difference between the volumes of the sliders before and after the fretting test. Results are shown in Table 1.

	UNWORN SPECIMEN	WORN SPECIMEN
V_{left} [mm³]	5,302	5,169
V_{right} [mm³]	5,198	5,070

Table 1 Volumes of the fixed specimen's sliders before and after the test

Thus, the whole worn volume lost from the fixed specimen $V_{loss,fix}$ was evaluated as the difference between the volume of the two sliders in the unworn condition $(V_{left}+V_{right})^{U,fix}$ and that in the worn condition $(V_{left}+V_{right})^{W,fix}$:

$$V_{loss,fix}= (V_{left} + V_{right})^{U,fix} - (V_{left}+ V_{right})^{W,fix} = 255{,}003\ \mu m \cdot mm2$$

Mobile specimen

The wear volume of the mobile specimen was estimated by measurements of peak and hole volumes in the contact area both in unworn and in worn conditions. Results are shown in Table 2.

	UNWORN SPECIMEN	WORN SPECIMEN
V_p [µm³]	7730161	13545247
V_h [µm³]	12221126	6246889

Table 2 Volumes of the peaks and holes in the contact surface of the fixed specimen before and after the test

Once the volumes of peaks V_p and holes V_h in the contact area were obtained both in worn and in unworn condition, the whole worn volume lost from the mobile specimen $V_{loss,mob}$ was computed as:

$$V_{loss,mob} = (V_{p,U} - V_{p,W}) + (V_{h,W} - V_{h,U}) = -11{,}789\ \mu m \cdot mm2$$

Thus, the total volume loss from the pair of specimens V_{loss} was obtained as:

$$V_{loss} = V_{loss,fix} + V_{loss,mob} = 243{,}214\ \mu m \cdot mm2$$

Even though the areas of contact were full worn, the volume estimated is negligible. The same result was obtained for every test.

Hence, it is concluded that for the given loading conditions and short test durations, no significant wear occurs on the analysed stainless steel specimens.

Chapter 6

6. Discussion and conclusions

A high frequency friction rig developed at LAQ AERMEC laboratory of Politecnico di Torino has been used to measure hysteresis loops under multiple loading conditions. Friction coefficient and tangential contact stiffness were extracted from hysteresis loops recorded and their trends were evaluated against normal load, sliding distance, wear and worn area of contact.

Results clarified some of the mechanisms and physics of frictional contacts. They have shown that:

- *Friction coefficient*:
  - It rapidly increases in the beginning of the test probably due to removal of oxide layers. After this “running-in period”, it still increases in time with a lower rate, reaching a steady state value.
  - It is mostly unaffected by normal load and relative displacement. This confirms that for dynamic simulations just a single value for the friction coefficient is required in the case of normal load and sliding distance variations.
- *Tangential contact stiffness*:
  - In mixed stick-slip and gross slip regime conditions its increase during a running-in period is probably due to an increased interaction between wear scars. The tangential contact stiffness reaches the steady state value

when the worn area does not increase anymore and the highest compliance between the two surfaces is attained.

    - In stick regime conditions, it is hypothesized that the increase in the contact stiffness is due to a plasticity hardening process occurring on the asperities subjected to continuous loading and unloading cycles.
    - It is confirmed that the tangential contact stiffness mainly depends on elastic deformation of asperities and bulk material.

      In fact, it increases with the normal load and it increases with the worn area of contact, probably due to resulting higher number of asperities in contact.
    - The tangential contact stiffness is also strongly dependent on the configuration of the worn area of contact. If the worn zones are spread over a large nominal area, the measured contact stiffness is lower.
    - The tangential contact stiffness reduces with sliding distance, probably due to the junction growth phenomenon described by Bowden and Tabor [39].

- *Wear volumes*:
    - A methodology has been proposed for an efficient and accurate estimation of the wear volume.
    - Results have shown that, for the given loading conditions and short test times, no significant wear occurs on the analysed stainless steel specimens.

Results of this research provide a better understanding of the physics of the contact parameters used in nonlinear dynamics simulations. In the future, it is suggested to perform more combinations of experiments and comparisons with different friction rigs, in order to generate better contact models that can be advantageously used to perform more accurate dynamics simulations.

Bibliography

[1] M. R. W. Brake, D. J. Ewins, and C. B. Wynn, “Are Joints Necessary? BT - The Mechanics of Jointed Structures: Recent Research and Open Challenges for Developing Predictive Models for Structural Dynamics,” M. R. W. Brake, Ed. Cham: Springer International Publishing, 2018, pp. 25–36.

[2] D. J. Ewins, “A Survey of Contact Hysteresis Measurement Techniques,” in *The Mechanics of Jointed Structures*, Springer, 2018, pp. 161–192.

[3] A. Fantetti *et al.*, “The impact of fretting wear on structural dynamics: Experiment and Simulation,” *Tribol. Int.*, vol. 138, no. May, pp. 111–124, 2019.

[4] R. B. Waterhouse, “Fretting Corrosion,” *Proc. Inst. Mech. Eng.*, vol. 169, no. 1, pp. 1157–1172, 1955.

[5] O. Vingsbo and S. Söderberg, “On fretting maps,” *Wear*, vol. 126, no. 2, pp. 131–147, 1988.

[6] O. Vingsbo, *Fretting and Contact Fatigue Studied with the Aid of Fretting Maps*. West Conshohocken, PA: ASTM International.

[7] D. Dowson, “History of tribology. London,” *Prof. Eng. Publ*, 1998.

[8] E. McCurdy, *The Notebooks of Leonardo Da Vinci, Complete*. Reprint Society, 1938.

[9] G. Amontons, “De la résistance causée dans les machines, Mémoires de l’Académie Royale A,” *Chez Gerard Kuyper*, pp. 1282–1699, 1699.

[10] C. A. Coulomb, *Théorie des machines simples en ayant égard au frottement de leurs parties et à la roideur des cordages*. Bachelier, 1821.

[11] N. P. Suh and H.-C. Sin, “The genesis of friction,” *Wear*, vol. 69, no. 1, pp. 91–

114, 1981.

[12] A. I. Vakis *et al.*, "Modeling and simulation in tribology across scales: An overview," *Tribol. Int.*, vol. 125, pp. 169–199, 2018.

[13] K. Kendall and D. Tabor, "An utrasonic study of the area of contact between stationary and sliding surfaces," *Proc. R. Soc. London. A. Math. Phys. Sci.*, vol. 323, no. 1554, pp. 321–340, 1971.

[14] J. Krolikowski and J. Szczepek, "Prediction of contact parameters using ultrasonic method," *Wear*, vol. 148, no. 1, pp. 181–195, 1991.

[15] R. S. Dwyer-Joyce and M. Gonzalez-Valadez, "Ultrasonic determination of normal and shear interface stiffness and the effect of Poisson's ratio," in *Tribology Series*, vol. 43, Elsevier, 2003, pp. 143–149.

[16] J.-Y. Kim, A. Baltazar, and S. I. Rokhlin, "Ultrasonic assessment of rough surface contact between solids from elastoplastic loading–unloading hysteresis cycle," *J. Mech. Phys. Solids*, vol. 52, no. 8, pp. 1911–1934, 2004.

[17] X. Shi and A. A. Polycarpou, "Measurement and modeling of normal contact stiffness and contact damping at the meso scale," *J. Vib. Acoust.*, vol. 127, no. 1, pp. 52–60, 2005.

[18] C. Siewert, L. Panning, A. Schmidt-Fellner, and A. Kayser, "The estimation of the contact stiffness for directly and indirectly coupled turbine blading," in *ASME Turbo Expo 2006: Power for Land, Sea, and Air*, 2006, pp. 841–853.

[19] M. Gonzalez-Valadez, A. Baltazar, and R. S. Dwyer-Joyce, "Study of interfacial stiffness ratio of a rough surface in contact using a spring model," *Wear*, vol. 268, no. 3–4, pp. 373–379, 2010.

[20] M. E. Kartal, D. M. Mulvihill, D. Nowell, and D. A. Hills, "Measurements of pressure and area dependent tangential contact stiffness between rough surfaces

using digital image correlation," *Tribol. Int.*, vol. 44, no. 10, pp. 1188–1198, 2011.

[21] G. Starzynski and R. Buczkowski, "Ultrasonic measurements of contact stiffness between rough surfaces," *J. Tribol.*, vol. 136, no. 3, p. 34503, 2014.

[22] A. Soom and C. I. Serpe, "Normal stiffness and damping at lightly loaded rough planar contacts," *Tribol. Int.*, vol. 100, pp. 171–177, 2016.

[23] M. Kreider and C. W. Schwingshackl, "Experimental evaluation of pressure dependent tangential contact stiffness," in *International Conference on Noise and Vibration Engineering*, 2018.

[24] M. Hashimoto, E. Marui, and S. Kato, "Estimation of contact stiffness at interfaces in machine structures by a beam model on an elastic foundation," *Tribol. Int.*, vol. 27, no. 6, pp. 423–431, 1994.

[25] B. W. Drinkwater, R. S. Dwyer-Joyce, and P. Cawley, "A study of the interaction between ultrasound and a partially contacting solid—solid interface," *Proc. R. Soc. London. Ser. A Math. Phys. Eng. Sci.*, vol. 452, no. 1955, pp. 2613–2628, 1996.

[26] P. Berthoud and T. Baumberger, "Shear stiffness of a solid–solid multicontact interface," *Proc. R. Soc. London. Ser. A Math. Phys. Eng. Sci.*, vol. 454, no. 1974, pp. 1615–1634, 1998.

[27] T. Fujimoto, J. Kagami, T. Kawaguchi, and T. Hatazawa, "Micro-displacement characteristics under tangential force," *Wear*, vol. 241, no. 2, pp. 136–142, 2000.

[28] R. S. Dwyer-Joyce, B. W. Drinkwater, and A. M. Quinn, "The use of ultrasound in the investigation of rough surface interfaces," *J. Trib.*, vol. 123, no. 1, pp. 8–16, 2000.

[29] J. Szwedowicz, M. Kissel, B. Ravindra, and R. Kellerer, "Estimation of Contact

Stiffness and its Role in the Design of a Friction Damper," in *ASME Turbo Expo 2001: Power for Land, Sea, and Air*, 2001.

[30] A. Baltazar, S. I. Rokhlin, and C. Pecorari, "On the relationship between ultrasonic and micromechanical properties of contacting rough surfaces," *J. Mech. Phys. Solids*, vol. 50, no. 7, pp. 1397–1416, 2002.

[31] S. Filippi, A. Akay, and M. M. Gola, "Measurement of tangential contact hysteresis during microslip," *J. Trib.*, vol. 126, no. 3, pp. 482–489, 2004.

[32] X. Shi and A. A. Polycarpou, "Investigation of contact stiffness and contact damping for magnetic storage head-disk interfaces," *J. Tribol.*, vol. 130, no. 2, p. 21901, 2008.

[33] M. Lavella and D. Botto, "Fretting wear characterization by point contact of nickel superalloy interfaces," *Wear*, vol. 271, no. 9–10, pp. 1543–1551, 2011.

[34] M. Lavella, D. Botto, and M. M. Gola, "Design of a high-precision, flat-on-flat fretting test apparatus with high temperature capability," *Wear*, vol. 302, no. 1–2, pp. 1073–1081, 2013.

[35] D. Botto, M. Lavella, and M. M. Gola, "Measurement of contact parameters of flat on flat contact surfaces at high temperature," in *ASME Turbo Expo 2012: Turbine Technical Conference and Exposition*, 2012, pp. 1325–1332.

[36] M. Lavella, "Contact Properties and Wear Behaviour of Nickel Based Superalloy René 80," 2016.

[37] W. D. Milestone and J. T. Janeczko, "Friction between steel surfaces during fretting," *Wear*, vol. 18, no. 1, pp. 29–40, 1971.

[38] D. K. Zhang, S. R. Ge, and Y. H. Qiang, "Research on the fatigue and fracture behavior due to the fretting wear of steel wire in hoisting rope," *Wear*, vol. 255, no. 7, pp. 1233–1237, 2003.

[39] F. P. Bowden and D. Tabor, “The Area of Contact between Stationary and between Moving Surfaces,” *Proc. R. Soc. Lond. A. Math. Phys. Sci.*, vol. 169, no. 938, pp. 391–413, 1939.

[40] L. Pesaresi, L. Salles, A. Jones, J. S. Green, and C. W. Schwingshackl, “Modelling the nonlinear behaviour of an underplatform damper test rig for turbine applications,” *Mech. Syst. Signal Process.*, vol. 85, pp. 662–679, 2017.

[41] F. P. Bowden and D. Tabor, “The friction and Lubrication of Solids.” Oxford University Press, Clarendon Press, pp. 5–17, 1986.